VEGF BOUND TO HEPARIN-CONJUGATED, ELECTROSPUN FIBRIN MICROFIBER SUPPORTS ECM FORMATION AND ORIENTATION ON 3D, *IN VITRO* MICROVASCULAR MODEL

By

Matthew Davenport

A thesis submitted to Johns Hopkins University in conformity with the requirements for the degree of Master of Science in Engineering

Baltimore, Maryland

August 2014

ABSTRACT

Current three dimensional (3D) models for microvasculature fail to understand the combinatorial role nanotopography, curvature, and bound growth factors have on extracellular matrix (ECM) deposition and cell alignment. Previous research shows that endothelial cell and ECM alignment is critical for managing shear stresses and contractile forces *in vivo*. We developed a novel, *in vitro* 3D model for microvasculature by using electrospun fibrin-alginate microfibers for endothelial cell proliferation and attachment with subsequent ECM deposition. Our preliminary studies showed that endothelial colony forming cells (ECFCs) cultured on our microfibers aligned in the direction of the stretched nanotopography. We found the ECM produced by ECFCs aligns perpendicular to the cell layer and circumferentially around the fibers themselves. The fiber diameter has a direct effect on ECM orientation, as fibers larger than 400 μm lead to random ECM orientations compared to the circumferentially wrapped ECM seen in 100 to 400 μm fibers. The endothelial layer is able to support the co-culture of vSMCs on our microfibers. Additionally, we successfully immobilized vascular endothelial growth factor (VEGF) on our fibrin system. We established a reductive amination protocol to conjugate fibrinogen to heparin, which is a known VEGF-binding molecule. The VEGF-bound fiber catalyzed ECM production without additional VEGF in solution, and also produced an ECM and cell orientation comparable to the stock fibrin microfibers. Summarily, we designed a dynamic, 3D fibrin-based platform for studying ECM deposition and cell interactions in-vitro in the presence of bound and unbound VEGF.

Advisor: Dr. Sharon Gerecht

Committee: Dr. Sharon Gerecht & Dr. Hai-Quan Mao

PREFACE

I leave Johns Hopkins after five inspiring and humbling years. I want to thank everyone at Johns Hopkins integral to my education and overall experience, from professors and administrators to family and friends.

First and foremost, I want to recognize my incredibly supportive family: Mom, Dad, Lisa & Brian, and Mike & Ellen. You have all been there for the triumphs and struggles, making sure I have the best chance to succeed in life, and I cannot thank you enough.

I would also like to thank Dr. Sharon Gerecht, Dr. Hai-Quan Mao, and the entire Gerecht Lab. Dr. Gerecht not only allowed me the opportunity to pursue cutting-edge research, but she showed me the importance of exploration, dedication, and curiosity. I want to thank Dr. Mao for the resources and knowledge essential to this project. Everyone in the Gerecht Lab (Kyung, Xin, Sravanti, Tom, Quinton, Maureen, Sebastian, Kim, and Greco) has made this an experience I am truly going to miss.

Lastly, I want to thank the rest of my friends and classmates that made my career at Hopkins more than just a degree. I have made some of my closest friends here, and you have all shown me the value of adventure and perspective. I want to especially acknowledge the Pi Kappa Alpha Fraternity and the Admissions Office.

LIST OF SYMBOLS AND ABBREVIATIONS

ECM	Extracellular matrix
ECFC	Endothelial colony-forming cells
VEGF	Vascular endothelial growth factor
PLGA	Polylactic-co-glycolic acid
FBS	Fetal bovine serum
vSMCs	Vascular smooth muscle cells
PES	Polyethersulfone
MWCO	Molecular weight cutoff (membranes)
TEM	Transmission electron microscopy
FN	Fibrin
HNMR	Proton nuclear magnetic resonance
AEMA	2-Aminoethyl methacrylate hydrochloride
EDC	Ethyl (dimethylaminopropyl) carbodiimide
NHS	*N*-Hydroxysuccinimide
ELISA	Enzyme-linked immunosorbent assay

TABLE OF CONTENTS

LIST OF FIGURES AND TABLES

INTRODUCTION

While there are hundreds of cancer types, one ubiquitous aspect of tumor formation is blood vessel formation, either through angiogenesis or vasculogenesis. Therefore, researchers are constantly working to define and inhibit the formation of vessels *in vivo* [1]. The aim of our research is to create a robust and adaptable model for microvascular vessels *in vitro* in order to understand the complex interactions between cells and environmental cues. We hoped our model, with the addition of specific progenitor cells, would shed light on the important ECM orientations and complexes during vasculogenesis.

Direct transfer of nutrients and oxygen is critical to the survival and proliferation of all mammalian cells, especially cancerous growths. A tumor's ability to metastasize or reach a critical size is directly influenced blood vessel invasion [1]. Judah Folkman, who conducted the first studies on angiogenesis in 1971, hypothesized an angiogenesis-dependent cancer model. From this point, cancer therapies began targeting angiogenic factors and precursors. Subsequent research showed that various stresses can lead to rapid changes in the "angiogenic switch," or the critical interaction between pro- and anti-angiogenic signals [2-4]. Such stresses include oxygen levels and pH (metabolic), inflammation (immune), and cell shear (mechanical), to name a few [5-6]. Angiogenesis' pervasiveness in cancerous tissue became the driving motivation for the research described herein.

One of the most important aspect of blood vessel organization is the extracellular matrix (ECM) and the specific alignment of ECM proteins. The ECM is the key component in the overall structural support necessary for angiogenesis. Additionally,

ECM proteins are responsible for the cellular and molecular signals that promote various stages of blood vessel formation, from initial lumen formation to final vessel stability. Therefore, the ECM possesses the ultimate control of angiogenesis, including structural support and scaffolding molecular signaling [7]. Essentially, the dynamic mechanisms of ECM formation is the controlling force behind all aspects of angiogenesis and blood vessel maturation.

Normal, adult blood vessels are formed by a primary, continuous basement membrane comprised mainly of laminins, collagen type IV, and proteoglycans [8-10]. The formation of this integral basement membrane is due largely in part to the recruitment of both endothelial cells and pericytes, the cells responsible for the deposition of ECM proteins [11]. While most blood vessels are found in the quiescent phase, angiogenesis and new vessel formation is directly stimulated through angiogenic cytokines [11-15]. The angiogenic response to these cytokines is as follows: (1) the basement membrane partially degrades in order to activate dormant endothelial cells; (2) the endothelial cells proliferate and generate a provisional ECM; (3) vascular tubes form through lumen generation and extension; (4) recruited pericytes cover the vascular tubes to finish the mature basement membrane. Previous studies have shown that interstitial collagen, along with other ECM proteins, support the key stages of angiogenesis [7].

Endothelial cells and their activation by cytokines and integrins is one of the most important precursors to successful angiogenesis. Endothelial cell's maximum survival and proliferation in the presence of multiple ECM protein components, showing that various proteins are likely to function cooperatively during angiogenesis [11-15]. Endothelial cell adhesion to the ECM is necessary for endothelial cell proliferation

because without adhesion, apoptosis is induced. Additionally, cell migration is induced after endothelial cell adhesion to the ECM, and migration is essential for angiogenesis [16].

Endothelial colony forming cells (ECFCs), endothelial progenitor cells, have shown the ability to both contribute to functional vessel formation and proliferate during this process [17-19]. ECFCs have a well-documented capacity for proliferation and blood vessel formation, making ECFCs the ideal cells for an in vitro vessel model. The ECFCs show similar characteristics of potent endothelial progenitor cells, and are used for *ex vivo* expansion to engineer vascularized tissue constructs in previous experiments [20-23].

Endothelial cells and pericytes not only respond to surface signals, they also detect and react to the nanoarchitecture of their microenvironment. Surface topography, more specifically line-grating features, has been shown previously to affect endothelial cell adhesion, alignment, and elongation. The endothelial cells are responsible for the production and orientation of the basal lamina, or the innermost lining of vascular walls [24-27]. In addition to the basal lamina, the tunica intima is composed of two more layers—subendothelial connective tissue and an internal elastic lamina. The tunica intima contains a variety of distinct, nanometer-sized ECM proteins. The subsequent layer is the tunica media, which includes mural cell ECM and is responsible for providing contractility during vasoreactivity. The final layer is the tunica adventitia and is found predominately in larger blood vessels [1, 29-35].

In addition to characterizing the individual ECM proteins, the orientation of the ECM fibrils plays a major role in the formation and integrity of mature blood vessels.

Research has shown that endothelial nuclei and cytoskeleton align with the direction of blood flow [35-37]. However, researchers have yet to characterize the orientation of microvasculature ECM. Previous studies focused mainly on larger vessels, such as the aorta and other large arteries. These studies indicate an organization of collagen that varies among all three layers of the vasculature, with specificity to vessel size and location [30-34, 38].

Studies of the larger vessels have shown that each tunica layer possess two different collagen fibril families with distinct orientations. In the adventitia, the outer layers show axial orientation compared to the circumferential alignment in the inner layers. The medial layer shows generally perfect circumferential order. More specifically, both elastic laminas tend towards a fenestrated orientation, but have shown axial and circumferential orientation in specific cases. The subendothelium is a multilayered fabric of collagen with distinct layers of longitudinal and circumferential fibrils [31-34].

Few research studies have attempted to characterize ECM alignment in smaller vessels. Thus far, three-dimension models for microvasculature have been difficult to recreate *in vitro* for the study of ECM deposition and alignment [39-41]. The majority of these studies utilized hydrogels [42-53], decellularized matrices [54-55], electrospun polymers [56-57], or vascular grafts [58-63]. Recent work is moving toward micropatterning that better controls vascular organization, because the aforementioned methods cause randomness in size, shape, and organization [64-66]. Overall, none of the models provide precise control over the topographical cues interpreted by cells. It is

these cues that produce specific vascular alignment and orientation necessary for cell-cell and cell-ECM interactions.

Tubular polymeric scaffolds provide a more viable option for studying microvasculature through a more refined platform. Previous tubular scaffolds have attained only millimeter diameters with limited mechanical strength [67-72]. In order to successfully model the microvasculature *in vivo* with a tubular scaffold, the platform must achieve a smaller diameter with sub-micron topography. The scaffolds must be biocompatible with specific cell adhesion, support cellular interactions, and exhibit sufficient mechanical properties [73].

Vascular endothelial growth factor (VEGF) has long been proven as a growth factor specific and critical for angio- and vasculogenesis. Currently, research has shown VEGF is not the only vascular endothelium-specific growth factor. The known growth factors include five in the VEGF family, four in the angiopoietin family, and one in the ephrin family. However, VEGF continues to act as the most critical driver of vascular formation due to its ability to initiate vasculogenesis or angiogenic sprouting. Additionally, VEGF is found to chemically signal the recruitment of monocytes after the deposition of an endothelial cell layer. [74]

Loading our fibrin microfiber model with immobilized growth factors, especially VEGF specific to angiogenesis, adds further functionality to the *in vitro* model. It has been shown that sustained and direct delivery of VEGF to the target cellular layers is necessary for the evolution and creation of mature blood vessels, both *in vivo* and *in vitro*. The two major factors in designing growth factor delivery systems—deliver a therapeutic concentration locally and sustain release over a substantial period of time. A

3D *in vivo* transplant of mature vessel networks, or fiber, would require the ability of VEGF delivery over an adequate time period. [74]

Previous studies have looked to delivery VEGF using a variety of 3D scaffolds, but fail to show sustained release from a tubular, fibrin matrix with specific nanotopography. It is not ideal for media dissolved delivery of VEGF because VEGF degrades quickly and does not necessarily localize at the correct receptor at the correct concentration. A bound growth factor has the ability to be administered directly to the endothelial cell layer at a desired concentration.

Researchers have encapsulated VEGF in a variety of nanoparticles and scaffolds. Poly(-lactic-co-glycolic acid) (PLGA) successfully encapsulates VEGF in both aqueous microspheres and rigid scaffolds. PLGA successfully protects degradation of VEGF in aqueous solutions, but PLGA is highly biodegradable, preventing sustained release over longer periods of time. PLGA scaffolds must be encapsulated by cell-culturing scaffolds, and cannot be chemically immobilized. Other VEGF delivery platforms, such as Matrigel and other hydrogels, successfully encapsulate and deliver VEGF over longer periods, but fail to have the high topographical specificity and tubular structure shown by fibrin microfibers. [75-77]

Heparin has a well-documented affinity for $VEGF_{165}$. $VEGF_{165}$ is the major VEGF isoform and generally the target of most VEGF immobilization and release studies. Heparin is also known to bind a variety of known growth factors. $VEGF_{165}$ is found to contain a heparin-binding domain. *In vivo*, the heparin binding domain allows these growth factors to localize directly to the high concentration of heparin sulfate in the

ECM. The heparin-binding domain comprises 55 residues but the subdomains at the N- and C-termini are poorly classified. [76, 78]

MATERIALS AND METHODS

Cell Culture

Human ECFCs (Lonza, Walkersville, MD) were used for experiments between passages 5 and 9. ECFCs were expanded in flasks coated with type I collagen (BD Biosciences, Franklin Lakes, NJ) in Endothelial Basal Medium-2 (EBM-2; Lonza) supplemented with EGM-2 Bulletkit (Lonza) and 10% fetal bovine serum (FBS; Hyclone, Logan, UT). ECFCs were fed every other day, passaged every 5 to 7 days with 0.05% trypsin/0.1% ethylenediaminetetraacetic acid (EDTA; Invitrogen, Carlsbad, CA). Human vSMCs (ATCC, Manassas, VA) were used between passages 4 and 9 and cultured in F-12K medium (ATCC) supplemented with 0.01 mg/ml insulin (Akron Biotech, Boca Raton, FL), 10% FBS (Hyclone), 0.05 mg/ml ascorbic acid, 0.01 mg/ml transferrin, 10 ng/ml sodium selenite, 0.03 mg/ml endothelial cell growth supplement, 10 mM HEPES, and 10 mM TES (all from Sigma-Aldrich, St. Louis, MO).

Preparation of normal 3D fibrin hydrogel microfiber

Fibrin hydrogel microfibers were generated by a new electrostretching method (**Fig. 1A**) (Zhang 2013). An aqueous solution of 1.5 wt% alginate (Sigma-Aldrich) was in-line mixed with 2 wt% fibrinogen (Sigma-Aldrich) at feeding rates of 2 ml/h and 1 ml/h, respectively. The mixed solution was then charged with 4 kV electric potential and extruded through a 25-gauge needle. The fibrinogen-alginate solution jet was collected at a distance of 3–5 cm from the needle tip, in a grounded, rotating bath (20 cm diameter, 20–40 rotation/min) containing 50 mM $CaCl_2$ solution with 5 units/ml thrombin (Sigma-Aldrich). To generate microfibers with different diameters, collection times were varied from 7–75 min. After spinning, the resulting ring of nanofibers was left in the collection

solution for 15 min before being cut once to obtain nanofiber strands. The crosslinked fibrin-alginate nanofibers were then soaked in 0.2 M sodium citrate overnight to remove calcium ions and dissolve alginate. Nanofibers were soaked in water for 30 min to remove sodium citrate, collected as an aligned bundle, stretched to 150% of their initial length, and air-dried for 30 min. Resulting microfibers (**Fig. 1A**) were wrapped around a custom-made plastic frame, then sterilized by soaking in 75% ethanol for 2 min followed by rinsing twice with sterile water. Microfiber diameter was measured from confocal z-stack projections.

Cell seeding and culture on fibrin hydrogel microfibers

ECFCs were seeded on microfibers of 15cm length total at a density of 4×10^5 cells/ml in 5 ml of ECFC media supplemented with 50 ng/mL of VEGF (Pierce, Rockford, IL, USA). The seeding tube was left on a tumbler (Labquake, Dubuque, IA) for 24 h at 37°C to facilitate cell attachment. Frames with ECFC seeded microfibers were then transferred to 35 mm Petri dishes using tweezers, and cultured in the same media in a CO_2 incubator at 37°C. Media was refreshed every other day thereafter. vSMCs were seeded on 5-7 day ECFC-seeded fibrin microfibers at $1\text{-}4\times10^5$ cells/ml in 5 ml of 0.5% serum or regular ECFC media, tumbled for 24 hours, and then transferred to 35 mm Petri dishes to continue culture. Media was changed every other day thereafter.

Preparation of 2D fibrin nanofiber sheets

Fibrin-alginate hydrogel nanofibers were prepared according to the same electrostretching protocol as described above. The collected fibrin-alginate hydrogel

nanofibers were wrapped around a modified plastic frame to form a sheet of nanofibers while slightly stretching the nanofibers to ensure proper alignment. The fibrin sheets were placed in a 0.2-M sodium citrate solution overnight to remove alginate, followed by a 30 min wash in water to remove excess sodium citrate. Fibrin sheets were then sterilized with 75% ethanol and rinsed twice with sterile water.

Cell seeding and culture on 2D fibrin sheets

Cells were seeded by placing 5×10^5 ECFCs in a concentrated solution of cells (about 2×10^6 cells/ml) directly on top of the fibrin sheet. After 5 min the cell solution that had filtered through the sheets was collected and reseeded on top of the fibrin sheets. This process was repeated 3 times, after which the same culture media as used for 3D fibers was added to the samples before being placed in a humidified incubator at 37°C in a 5% CO_2 atmosphere. Media was refreshed every other day up to 5 days of culture.

Preparation of 3D polyethersulfone (PES) fibers

Solid polymer fibers were prepared as a control according to a modified electrostretching protocol. In brief, PES (Goodfellow Cambridge Limited, UK, Mw 55,000) was dissolved in 30 wt% DMSO and electrospun under an electric potential of 5 kV. The feed rate of PES solution was 12 ml/h to initiate a polymer jet, which was collected in a grounded, rotating ethanol bath (20-40 rotations/min) to extract the solvent. The collection distance was set to 5 cm. After 10 min in ethanol, PES strings were removed from the bath and air dried. After electrospinning, PES fibers were wrapped around a seeding frame similarly to the fibrin hydrogel microfibers. Samples were then plasma-treated for 5 min before soaking for 5 min in a 10 units/ml thrombin in 15 mM

$CaCl_2$ solution. Thrombin-coated PES fibers were then immersed in a 0.2% fibrinogen solution diluted in 0.9% NaCl for fibrinogen polymerization into fibrin. Excess fibrin coating on the frame and outside of the fibers was removed before sterilization with 75% ethanol for 1-2 min. Samples were rinsed twice with sterile water, after which cell seeding was performed similarly to the fibrin microfibers as described above.

Plasminogen degradation of fibrin microfibers

Plasminogen was dissolved in distilled water based on the batch's unit per mg calculation to keep activity constant. We seeded ECFCs using the aforementioned coverslip seeding protocol and cultured placed in a humidified incubator at 37°C in a 5% CO_2 atmosphere. Media was refreshed every other day up to 5 days of culture. The cells were cultured with the correct concentration of plasminogen in either DMEM base media (Lonza) or the previously described ECFC normal media.

Cell viability assay: calcein staining

Cells were washed in PBS and stained using 0.5 mL of 2 μM calcein and 4 μM in sterile PBS. Staining was carried out for 45 minutes at room temperature kept away from light. All future live/dead staining was carried out in this manner.

Preparation of thiolated fibrinogen with Ellman's Assay

Thiolated fibrinogen stock was created by dissolving 10mg/mL fibrinogen into 0.9% NaCl solution. 0.05 grams of Traut's Reagent (2-Iminothiolane hydrochloride) per gram of dissolved fiobrinogen was added. The solution incubated at room temperature for 15 hours. The fibrinogen was dialyzed using 3500 MWCO membrane against 5 mM

HCl for 24 hours and against 1 mM HCl for the next 24 hours. The final dialysis was against 0.9% NaCl solution. The thiolated fibrinogen was frozen at -80°C and lyophilized using vacuum freezer for roughly 72 hours. To determine the concentration of free thiols on fibrinogen, Ellman's Assay for free thiols was carried out. 1mg/mL of thiolated fibrinogen was dissolved into 0.1 M sodium phosphate buffer (pH 8.0). The Ellman's reagent consisted of 4 mg/mL of DTNB (5,5'-dithiobis-(2-nitrobenzoic acid)) dissolved into the same phosphate buffer. The $DTNB_r$ reference cuvette consisted of 100 µL of DTNB and 100 µL of phosphate buffer. The phosphate buffer reference cuvette contained 200 µL of 0.1M phosphate buffer. The sample cuvettes contained 100 µL of DTNB reagent and 100 µL of thiolated fibrinogen solution. The absorbance of all cuvettes was read at an experimental wavelength of 412nm and a reference wavelength of 630nm using a UV spectrophotometer.

Preparation of methacrylated heparin with HNMR assay

Methacrylated heparin was prepared by first dissolving 1.0% (w/v) heparin sodium salt into 50 mM MES (2-(*N*-morpholino)ethanesulfonic acid) buffer (pH 6.5) with 0.5M NaCl. NHS (*N*-Hydroxysuccinimide) and EDC (ethyl (dimethylaminopropyl) carbodiimide)) are added in a 1:1:2 heparin:NHS:EDC molar ratio. After five minutes, added *AEMA (*2-Aminoethyl methacrylate hydrochloride) in 1:2:1 NHS: EDC: AEMA molar ratio for 24 hours at room temperature. After 24 hours, methacrylated heparin precipitated using excess acetone at 4°C for longer than 2 hours. The precipitate is centrifuged at 10g for 10 minutes to pellet the methacrylated heparin. The excess acetone is precipitated and the pellet is air dried. The methacrylated heparin is dissolved to 1% (w/v) in dH_2O. The methacrylated heparin solution is dialyzed, using 3500 MWCO

membrane, against distilled water for three days with daily water changes. The solution is frozen at -80°C and lyophilized with a vacuum freeze dryer. To confirm methacrylation, the heparin is dissolved in D_2O at 10mg/mL. [79]

2D crosslinking and heparin fluorescent labeling

Heparin was fluorescently labeled using Lightning-Link Rapid DyLight 550 conjugation kit. The kit is typically used for antibody labeling but is also used for labeling of peptides. The standard protocol was followed but the labeling step was carried out overnight at room temperature. 75 µL of 3 mg/mL methacrylated heparin in PBS was added to 7.5 µL of modifier and added to the lyophilized fluorescent label. The solution was quenched for five minutes.

For crosslinking, 250 µL of one percent thiolated fibrinogen solution in water was evenly spread on a standard 12-well culture plate. The fibrinogen was cleaved to fibrin using 250 µL of 10 units thrombin in order to set the fibrin layer. 10 µL of 3 mg/mL fluorescently labeled heparin was added and left to incubate at room temperature for 30 minutes. After conjugation, the fibrin was washed three times with dH_2O without disrupting the matrix. For control, the thiolated fibrinogen was replaced with stock fibrinogen.

Preparation of heparin bound fibrin using reductive amination

Heparin was bound to fibrin by dissolving 10 mg/mL of fibrinogen into 0.1 M sodium tetraborate and 0.4 M NaCl. After a complete dissolve, a 25:1 molar ratio of heparin sodium salt was added to the fibrinogen solution. This solution was mixed for one hour. The solution is reduced by Schiff base by adding sodium cyanoborohydride

($NaCNBH_3$) in 50 molar excess. The reaction proceeded for 24 hours at room temperature. The solution is dialyzed using a 6000-8000 MWCO membrane against distilled water. The solution is frozen at -80°C and lyophilized using a vacuum freeze dryer. To remove the brown color, the solution is filtered through a 0.22 μm syringe filter. [80]

Preparation of heparin bound 3D fibrin hydrogel microfiber

Heparin bound fibrin hydrogel microfibers were prepared using a similar electrospinning procedure as mentioned previously for the stock fibrinogen solutions. However, the fibrinogen-based solution consisted of filtered heparin conjugated fibrinogen at 4 wt% in 10% PEO. The feeding rates are at 2 mL/h fibrinogen-heparin and 1 mL/h of 1.5 wt% alginate. The electrospinning process followed the same parameters as outlined previously, but only five minutes of spin and the thrombin was increased to 10 units/mL. Additionally, the fibers were stretched to 125% of its original length to account for excess fragility. The wrapping and seeding process is identical to the stock fibrinogen solution. However, for seeding cells, we used normal ECFC media after tumbling in high-VEGF ECFC media for 12 hours.

ELISA assay for VEGF release

Modified heparin fibers were created using aforementioned reductive amination and electrospinning protocol. ELISA conducted using VEGF Human ELISA kit (Invitrogen) with the standard protocol and standard curve from VEGF used in previous experiments. Prepared fibers were wrapped on plastic frames similar to culture conditions and placed in 2mL of water with 50ng of VEGF in 12 well culture dish in a 37C incubator. At each time point, I removed 100 microliters of solution and replaced

with 100 microliters of DI water to keep volume constant. Percent release calculated from starting concentration for each sample (100%) and graphed in GraphPad.

Immunofluorescence staining and confocal microscopy imaging

Cell-microfiber constructs were fixed with 3.7% formaldehyde (Fisher Chemical, Fairlawn, NJ) for 15 min, permeabilized with 0.1% Triton X-100 solution (Sigma-Aldrich) in 3.7% formaldehyde for 10 min, washed three times with PBS, and incubated for 1 h at room temperature with the indicated primary antibodies (**Appendix 1**). After rinsing with PBS three times, samples were then incubated with the appropriate secondary antibodies or conjugated phalloidin (**Appendix 1**) at room temperature for 1 h. Samples were then rinsed with PBS three times, and counterstained with DAPI for 10 min. Z-stack and cross-sectional images were obtained and processed using confocal microscopy (LSM 510 Meta, Carl Zeiss Inc., Thornwood, NY). Epifluorescence images were obtained using an Olympus BX60 microscope.

Transmission electron microscopy

Samples were prepared for transmission electron microscopy (TEM) analysis as described previously (Hanjaya-Putra, Bose et al. 2011). Briefly, samples were fixed with 3.7% formaldehyde, 1.5% glutaraldehyde in 0.1 M sodium cacodylate, 5 mM $CaCl_2$, and 2.5% sucrose at room temperature for 1 h and washed 3 times in 0.1 M cacodylate / 2.5% sucrose (pH 7.4) for 15 min each. The cells were post-fixed with Palade's OsO_4 on ice for 1 h, *en bloc* stained with Kellenberger uranyl acetate overnight, dehydrated through a graded series of ethanol, and then embedded in EPON. Sections of 80-nm were cut,

mounted onto copper grids, post-stained in 2% uranyl acetate and Reynolds lead citrate, and viewed using a Phillips EM 420 transmission electron microscope (FEI). Images were captured with an Olympic Soft Imaging Systems Megaview III CCD digital camera.

Scanning electron microscopy

Hydrogel microfiber samples were first serially dehydrated in 50%, 60%, 70%, 80%, 90%, 95% and 100% ethanol for 15 min in each solution, critical point dried, and then sputter-coated with 8-nm thick Au/Pd. Samples were imaged on a field-emission SEM (JEOL 6700F, Tokyo, Japan).

Image and statistical analyses for unmodified fibrin

All image analyses were performed on at least 60 measurements per condition. Cytoskeletal alignment angle was calculated by fitting an ellipse to each cell using the LSM 510 software and measuring the angle between the long axis of each ellipse and the longitudinal axis of the microfiber, found by drawing a line at the edges of the microfiber in its image projection. ECM angle of orientation was measured by drawing a line following the ECM deposition and finding the angle between the line and the longitudinal axis of the microfiber. Graphs were plotted with 5-95% confidence intervals. Unpaired two-tailed Welch-corrected *t*-tests were performed where appropriate (GraphPad Prism 5.01, GraphPad Software, San Diego, CA). Significance levels were determined between samples examined and were set at $*p < 0.05$, $**p < 0.01$, and $***p < 0.001$.

Image and statistical analyses for modified fibrin with VEGF

All images were analyzed and optimized using LSM 510 software. Cell viability assays were calculated using ImageJ 1.47v particle analyze with counting. Theoretical HNMR curves created using ChemDraw and with GraphPad Prism 5.01 utilized for experimental HNMR data. Images in Figure 10 were rendered and imaged using the same methods as unmodified, 3D heparin with LSM 510 software.

RESULTS

Unmodified fibrin microfiber properties with ECFC attachment

Our main focus of this project was the development of both a stock fibrinogen and a heparin-fibrinogen conjugated microfiber. We employed a novel approach that aligned thrombin cross-linked microfibers to create a specific topography with specific characteristics. The internal and topographical nano-alignment is integral to the subsequent cellular experiments. We specifically controlled the alignment and polymer chain alignment using the electrical field, stretching, and mechanical spinning. Additionally, we could uniformly control the diameter of individual fibers by using a varying concentration of fibrinogen or spin time.

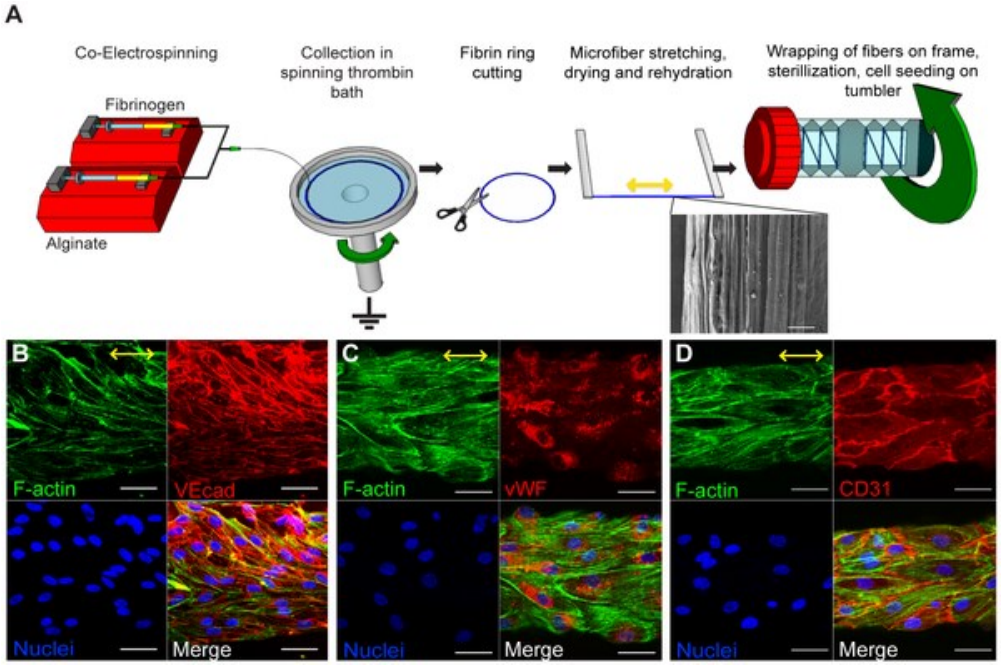

Figure 1. Preparation of fibrin hydrogel microfibers with preliminary ECM attachment. (A) Schematic of the preparation of fibrin hydrogels, from electrospinning to ECFC seeding with tumbling. SEM of critical-point dried fibrin microfiber with aligned surface topography (10µm scale bar). The drawing is not scale. (B-D) Confocal z-stack image projections of ECFCs seeded on fibrin hydrogel microfibers showing horizontal alignment after five days in culture. F-actin (phalloidin) is shown in green, EC-specific markers in red, and nuclei in blue. The yellow arrows show the alignment of the fibrin nanotopography and stretching during formation. The scale bar is 50 µm. n≥2 per stain with quadruplicates. PLoS ONE 8(11): e81061. doi:10.1371/journal.pone.0081061

Figure 1A diagrams the electrospinning process from the base syringe solutions to the stretching and drying step. We confirmed the proposed longitudinally aligned nanotopography using scanning electron microscopy of a critical-point dried fibrin fiber. The topographical features are shown to fall between 1 μm and 100 nm, which the optimal range for endothelial adhesion, migration, and orientation [24-27].

We wanted to demonstrate the adhesion and morphology of ECFCs on the stock fibrin microfibers. For the seeding of ECFCs, we added the cell culture in high VEGF media to the fibers using 24 hours of continuous, gentle rotation to ensure proper cell distribution and even attachment. We observed sufficient seeding after 24 hours. After five days in culture with two day high-VEGF media changes, we observed continuous ECM wrapping in addition to elongated and longitudinally aligned ECFCs as indicated by the F-actin staining in **Figure 1B-D**. ECFCs seeded on the fibers expressed normal membrane markers (VEcad & CD31) and cytoplasmic markers (vWF), indicating proper adhesion and maintenance of ECFCs.

Alignment of ECFC deposited ECM on stock fibrin

We strived to characterize and study the ECM production by ECFCs. In previous work, we documented ECFC's ability to produce collagen IV, fibronectin, and laminins when cultured on collagen-coated 2D coverslips [82]. In **Figure 2A**, we show that ECFCs similarly deposit collagen IV, laminin, and fibronectin after one day culture on our novel hydrogel microfibers. By day five, ECFCs produce a continuous layer with an abundance of ECM coating **(Fig. 2B.)** We noticed that the ECM proteins deposited by ECFCs under these conditions wrap circumferentially around the microfibers. This ECM

was perpendicular to the endothelial orientation **(Fig. 2C.)** ECFCs failed to deposit collagen I, but the ECM deposited is found to exist below or within the ECFC layer **(Fig. 2E.)**

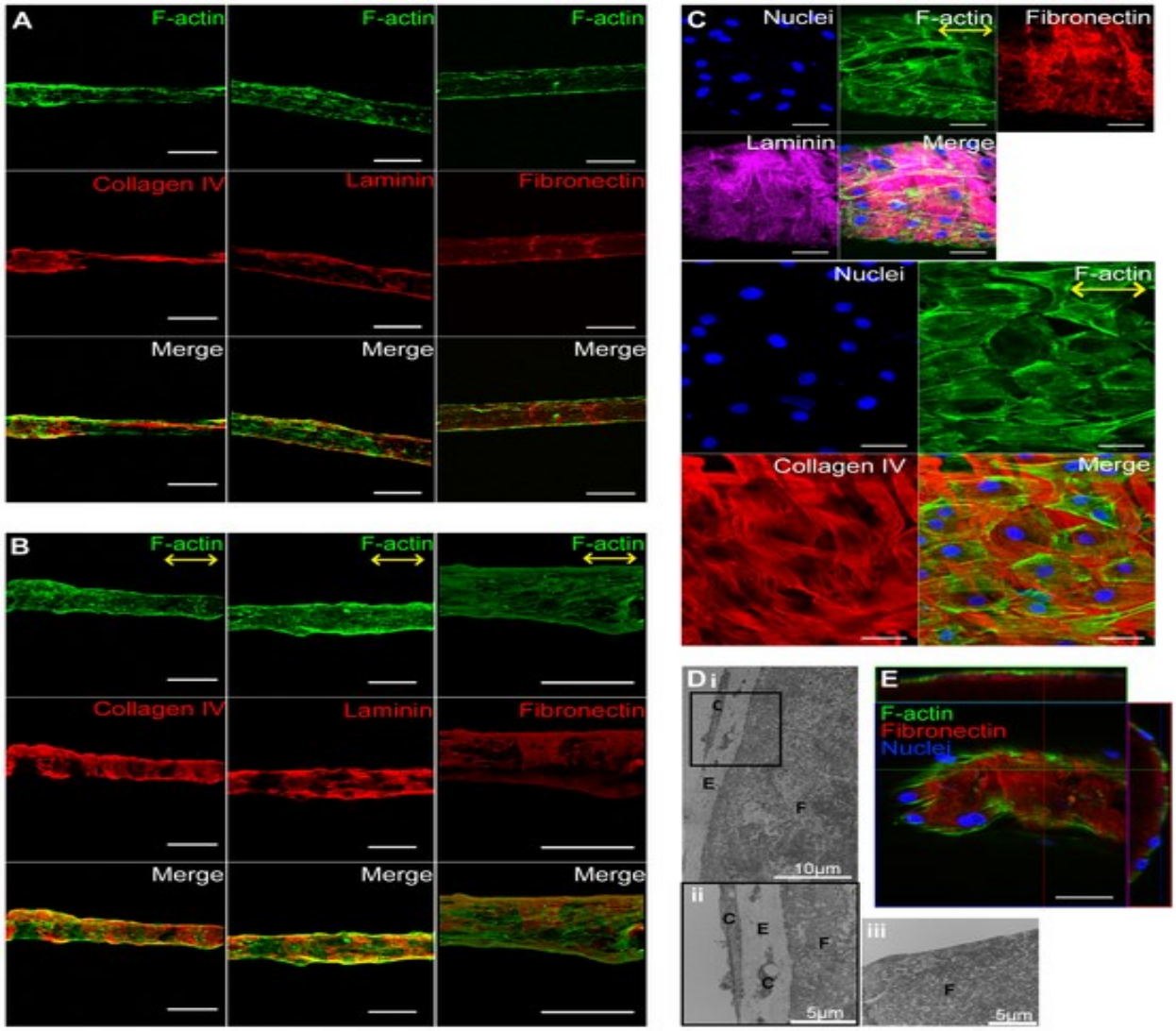

Figure 2. ECM deposition by ECFCs on 3D fibrin microfiber.
(A) Confocal z-stack image projections of ECFCs seeded on stock fibrin microfibers after one day. (B) Confocal z-stack image projections of ECFCs seeded on stock fibrin microfibers after five days. The scale bars are 200 μm. (C) High magnification (40X objective) confocal image projections of laminin (magenta), fibronectin (red) and collagen IV (red) with distinct fibrin wrapping of ECM proteins. F-actin stained in green to show cell alignment and nuclei in blue for cell coverage. (D) TEM images of cross-sectional slices of fibrin microfiber under five day culture conditions (i-ii) with cells and (iii) without cells. The labels indicate fibrin, "F," ECM, "E," and cells, "C." (E) Cross-sectional projections of confocal z-stack images of 5 day ECFC culture on stock fibrin microfibers. The ECM proteins are stained red, F-actin green, and nuclei blue. (A) n≥2 (B-E) n≥5 with quadruplicates, per stain. . PLoS ONE 8(11): e81061. doi:10.1371/journal.pone.0081061

3D polyethersulfone (PES) and 2D fibrin sheet controls

We wanted to show that the circumferential ECM wrapping is induced by the specific nanotopography of the fibrin 3D microfiber. As previously mentioned, line-grating topography is purported to influence endothelial cell adhesion, alignment and elongation [24-27]. We wanted to seed cells on two control materials to determine the influencing factors in ECM deposition. First, we seeded ECFCs on flat, 2D fibrin sheets with the same aligned nanotopography as the 3D microfibers, but without the curvature and dimensionality. As hypothesized, the cells and actin filaments followed the topographical alignment of the 2D sheets. However, the deposition of the ECM proteins, such as collage IV, fibronectin and laminins, was random and showed no visible alignment **(Fig. 3A.)** This is in direct contrast to the ECM deposition on 3D fibers, which aligned circumferentially and perpendicular to the cell alignment and nanotopography. This result indicates that not just the microfiber nanotopography, but the geometry as well, may play a specific role in regulating ECM alignment.

For the second control, we utilized similarly electrospun PES microfibers with the same dimensionality and geometry as the experimental fibrin microfibers. However, the PES fibers do not possess the aligned nanotopography. To maintain the biocompatibility and bioadhesiveness of the fibrin fibers, we used a fibrin coating over the PES fibers for better ECFC attachement and proliferation. We calculated the PES fibers to have a diameter in the range of 240 ± 45 μm, which is consistent with the diameters of the fibrin microfibers. Therefore, the fibrin-coated PES is a sufficient model for studying the effect of aligned nanotopography on ECM deposition. We seeded ECFCs on the PES fibers using the same protocol as the fibrin microfibers and visualized the ECM after a five day

culture. The ECFCs fully covered the PES microfibers and deposited ECM after five days. The ECFCs and F-actin alignment was not completely random, but showed a slightly diagonal orientation to the fiber's horizontal axis. The ECM, however, deposited circumferentially around the PES fiber perpendicular to the horizontal axis, similar to that of the fibrin microfiber **(Fig. 3B.)** For both cases, the angle between the ECM protein fibrils and the fiber's longitudinal axis centered around 90° **(Fig. 3C-D.)** Additionally, the deviation from 90° was small, indicating a small distribution of ECM alignment **(Fig. 3E.)**

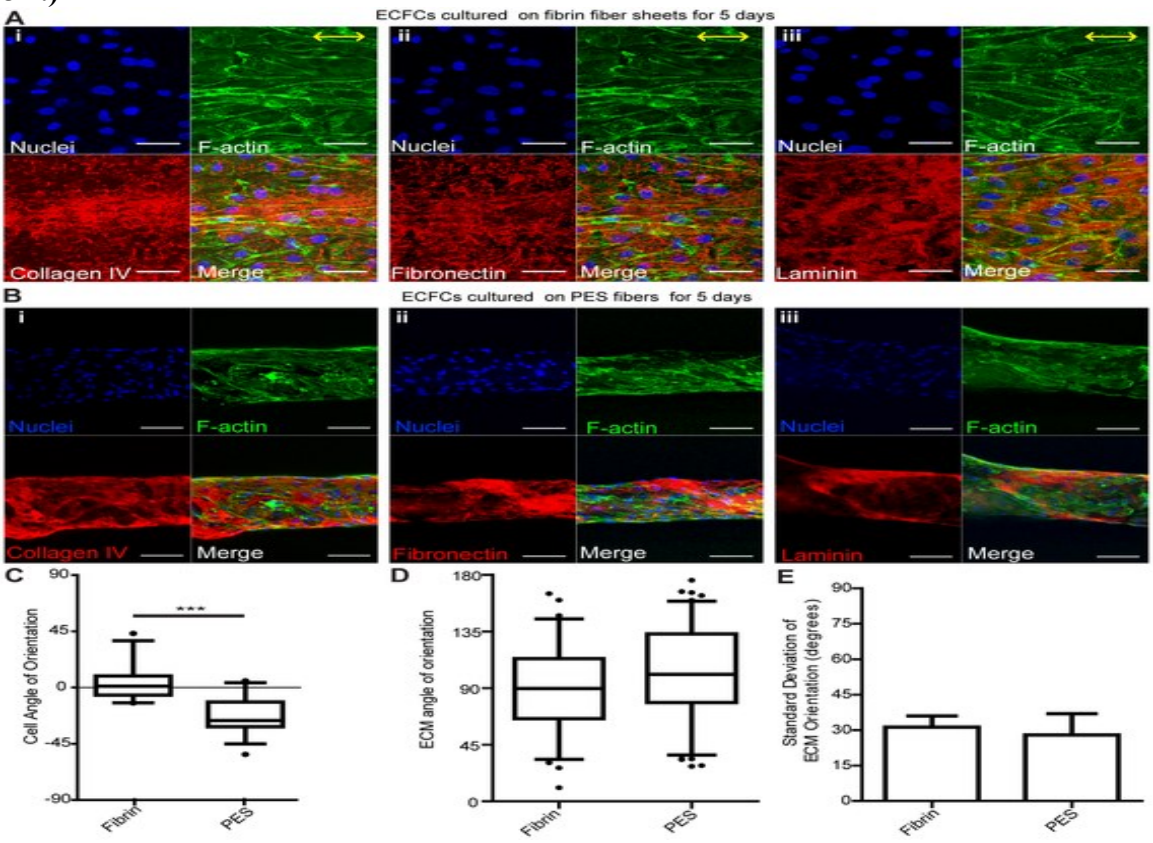

Figure 3. ECFCs cultured on 3D PES and 2D fibrin sheet controls with ECM orientation. (A) Confocal z-stack image projections of ECFCs cultured on 2D fibrin sheets for 5 days. The yellow arrows show the direction of the nanotopography, and scale bars are 50 μm. (B) Confocal z-stack image projections of ECFCs cultured on 3D fibrin-coated PES fibers for five days. The scale bars are 100 μm. F-actin is stained in green, ECM proteins in red, and nuclei in blue. Box-and-whisker plots showing ECFC (C) and ECM (D) angle of orientation on PES and fibrin hydrogel microfibers after 5 days in culture. (E) Standard deviation of ECM angle of orientation. Error bars represent 5–95% confidence intervals. Significance levels in the mean represented by ***p<0.001. (A)n≥2 in duplicates (B)n≥4 in quadruplicates (C)n≥2 with quadruplicates. PLoS ONE 8(11): e81061. doi:10.1371/journal.pone.0081061

Curvature dependence on ECM alignment

The results of this study indicates that ECM organization is more dependent on the geometry of the microtubular structure than the alignment of the cultured ECFCs. We hypothesized that the microfiber diameter, and thereby the curvature, was the key factor in determining ECM alignment. To test this theory, we created four sizes of fibrin microfibers (107.1±11.7 μm, 136.1±12.1 μm, 372.0±27.3 μm, and 443.4±30.6 μm) for the study of ECM orientation. These fibers exhibited the same nanotopographical alignment as demonstrated previously by the smaller fibers.

Due to the similar topography across all fiber diameters, the ECFCs and F-actin aligned in the direction of the fiber topography. However, as the fiber size increased, the ECM fibril perpendicular orientation decreased **(Fig. 4A.)** We measured the angle of ECM (collagen IV) alignment in relation to the microfiber's longitudinal axis. For all fibers under 400 μm, the average angle was 90° with small deviation from the mean. However, the largest fiber (443.4±30.6 μm) showed a much more random orientation with a spread distribution. This large distribution ranging from 0° to 180° is indicative of a non-circumferential, random pattern of ECM deposition by ECFCs. The largest microfibers led ECM angles with the highest standard deviation compared to smaller microfibers **(Fig. 4B-C.)** Additionally, collagen nano-fibrils are shown to the follow the same circumferential alignment at the nano-scale. However, the collagen nano-fibrils did not have specific nano-scale orientation when deposited on the larger fibers.

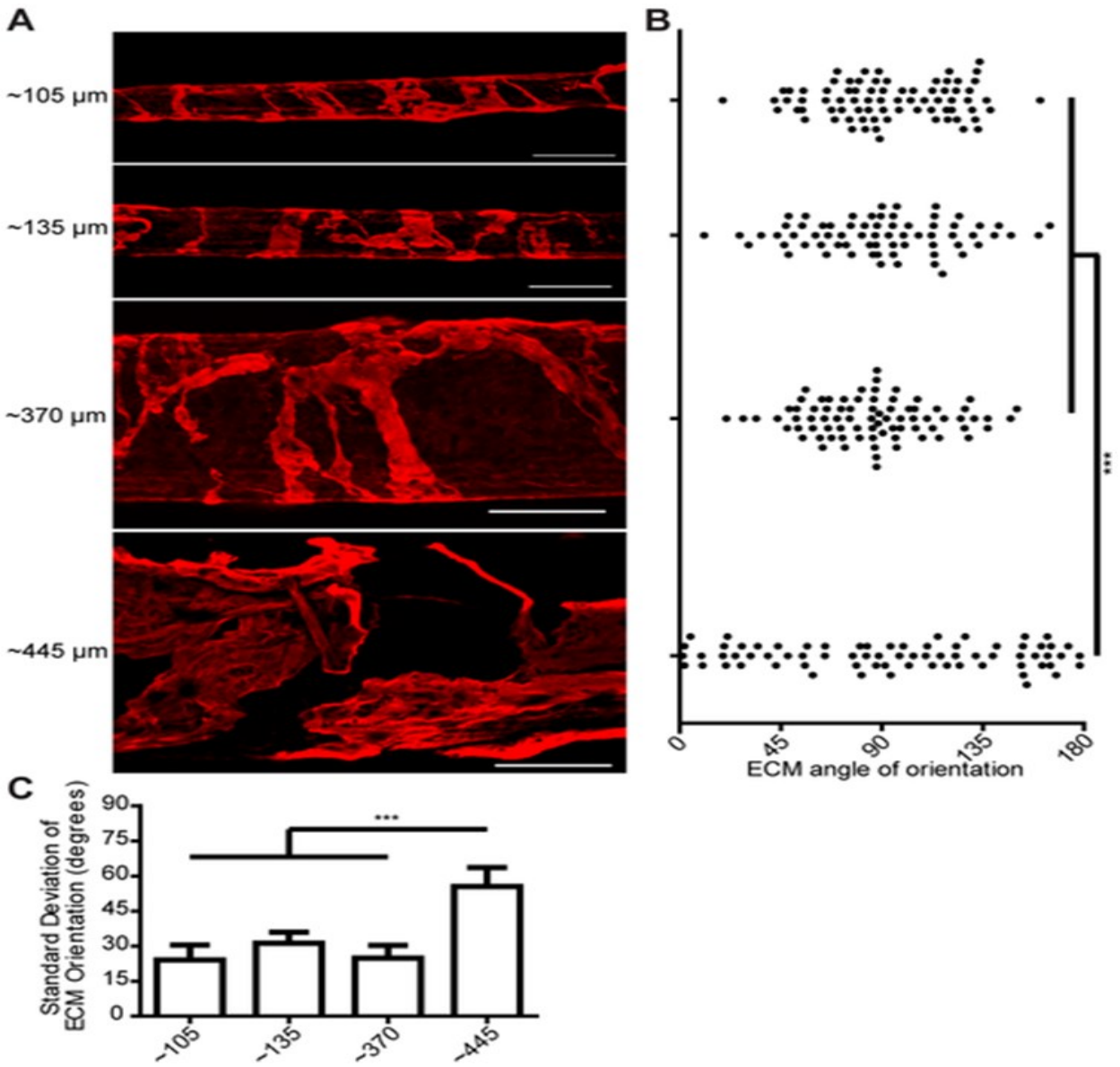

Figure 4. ECFC deposited collagen orientation depends on fibrin microfiber curvature. (A) Confocal z-stack image projection of collagen IV (red) deposited on fibrin microfibers with increasing diameters (105 µm to 445 µm.) Scale bars are 200 µm. (B-C) Scatter plot and standard deviation of ECM angle orientation compared to microfiber diameter. Error bars represent 5-95% confidence intervals. Significance levels in the distribution represented by ***p<0.001. n = 2 with quadruplicates. PLoS ONE 8(11): e81061. doi:10.1371/journal.pone.0081061

vSMC co-culture on ECFC seeded fibrin microfibers

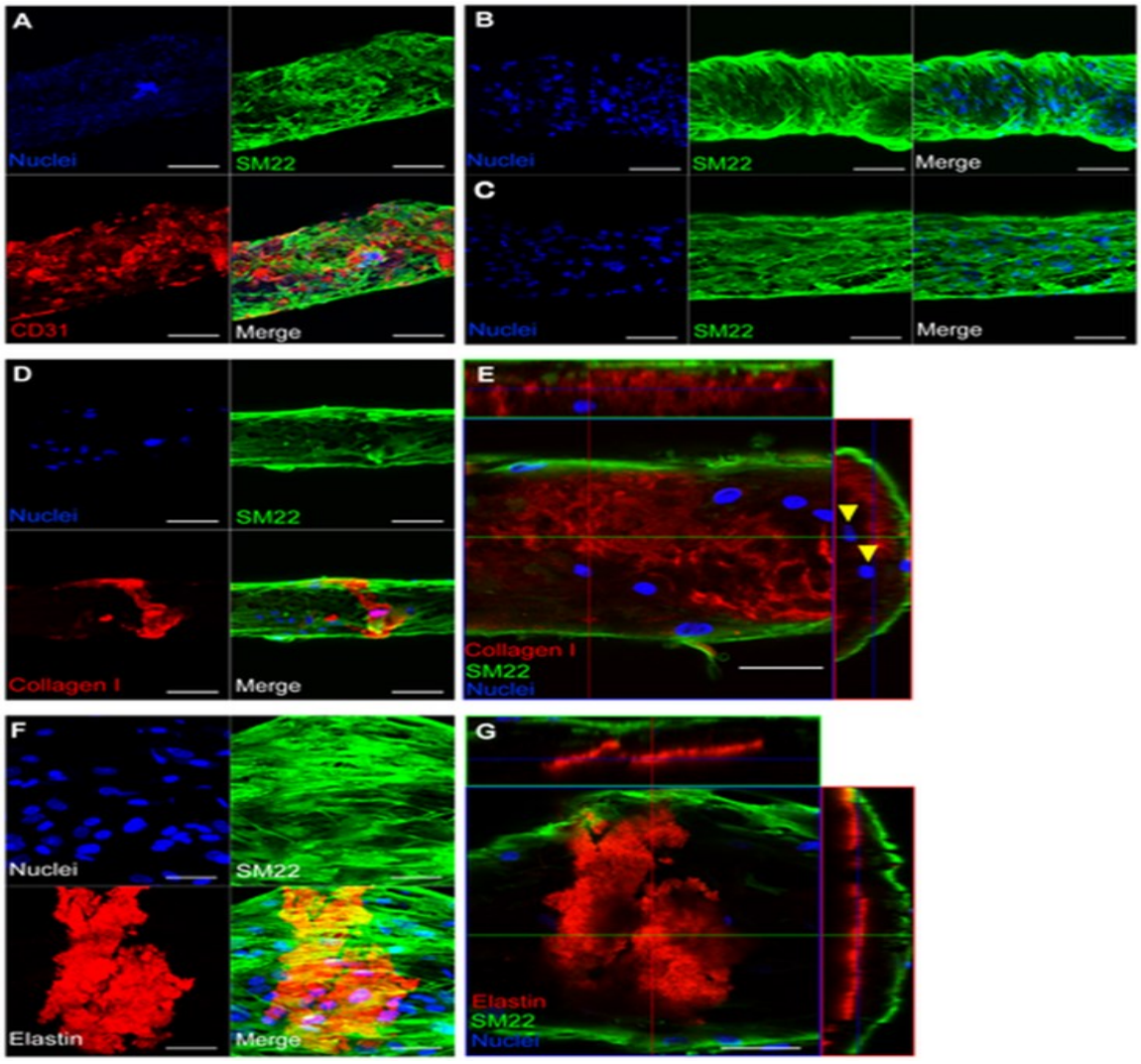

Figure 5. vSMCs co-cultured on ECFC produced ECM.
Confocal z-stack image projections of fibrin microfibers seeded with ECFCs followed by (A) co-culture of vSMCs for 2 days. Scale bars are 200 μm. Co-cultured vSMCs for 3 days showing (B) wrapping and (C) aligned arrangement. Scale bars are 100 μm. (D) Collagen I deposited by co-cultured vSMCs after 3 days in co-culture. Scale bars are 100 μm. (E) Cross-sectional projection of confocal z-stack images of vSMCs after 5 days in co-culture. The yellow arrowheads indicate the presence of SM22 negative cells. Scale bars are 50 μm. (F) Confocal z-stack image projection and (G) cross-sectional projection of co-cultured vSMCs after 5 days in co-culture. Scale bars are 50 μm. SM22 is shown in green, CD31 in red, collagen I and elastin in red, and nuclei in blue. (A, F) n=2 in quadruplicates. (B-E) n≥3 with quadruplicates.
doi:10.1371/journal.pone.0081061.g006

One of the unique aspects of our model is the ability to co-culture different cell types simultaneously. We looked at the interaction of vSMCs with the ECFC layer and

the ECFC deposited ECM. We show that ECFCs seeded on fibrin microfibers allow the culture, proliferation, and attachment of vSMCs **(Fig. 5A.)** vSMCs were found to deposit collagen I and elastin about the ECFC layer after 3 and 5 days above the SM22-negative cellular layer **(Fig. 5D-F.)** The vSMCs showed cellular alignment with the longitudinal axis of the fibrin microfibers, but the ECM showed both random and circumferential alignment **(Fig. 5B-C.)**

Plasminogen degradation of fibrin microfiber

An important characteristic of fibrin is its ability to be degraded by plasminogen. Plasmin is able to enzymatically cleave various portions of the fibrin mesh and create small fibrin pieces for easy removal. The process is known as fibrinolysis. For our application, the degradation of fibrin allows us to create a hollow cell-ECM structure to be eventually used to test a variety of parameters, including leakiness, blood flow capacity, and response to shear stress. A hollow cellular structure (ECFCs and vSMCs) with continuous ECM would further increase the importance of the model. Our previous studies have shown that plasminogen degrades fibrin in a relatively short time period, but we have yet to study the plasminogen's effect on cells, especially the somewhat sensitive ECFCs. To test this effect, we cultured ECFCs on 2D collagen-coated coverslips for five days when the cells reach sixty percent confluence. We used both traditional ECFC media and DMEM base media to test previously utilized plasminogen concentrations on cell viability. The live/dead calcein stain shows that the cells responded negatively for all concentrations of plasmin and for the DMEM control. The images show a larger population of dead cells (red) under these conditions **(Fig. 6A-B.)** As expected, the control coverslips with normal ECFC media show a majority of live cells (green.) We

used a higher concentration of plasminogen in the ECFC media because the increased serum level in ECFC media inhibits the activity of plasminogen in solution.

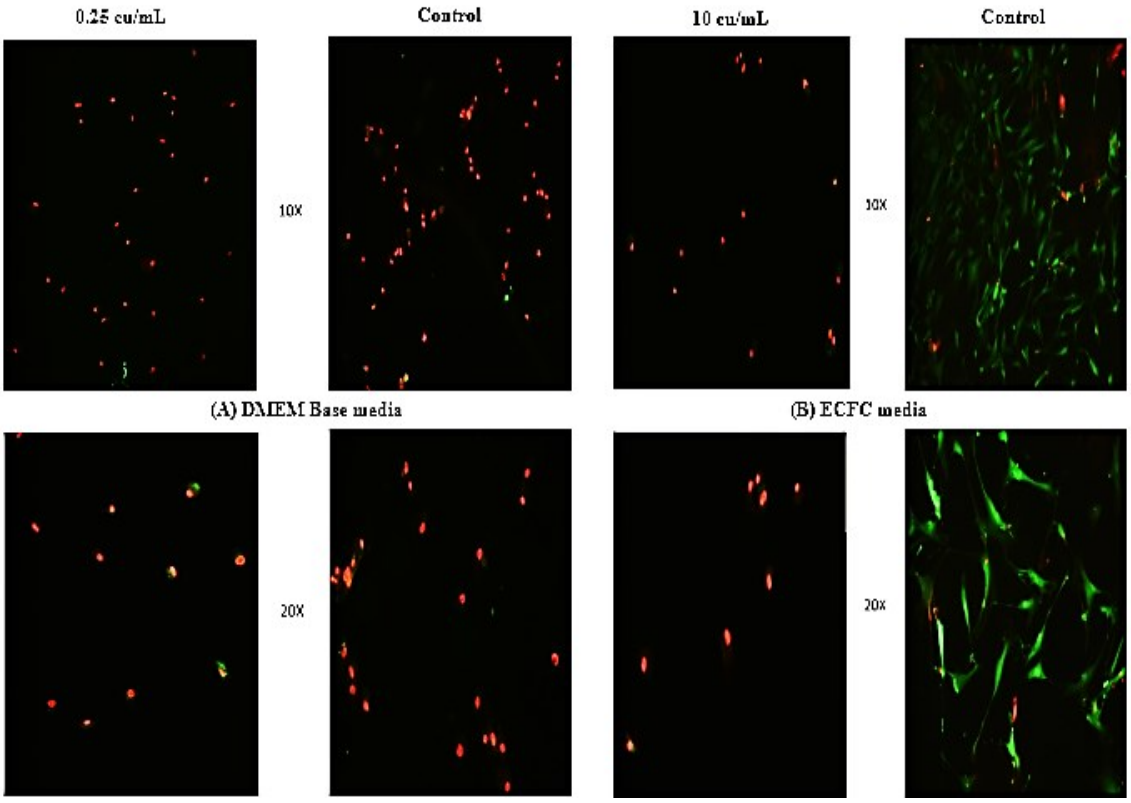

Figure 6. ECFC viability in the presence of aqueous plasminogen on 2D coverslips.
2D fluorescent images of ECFCs cultured in (A) DMEM base media with 0.25 cu/mL plasminogen and (B) ECFC media with 10 cu/mL plasminogen. The cells are stained with 2μM calcein (live/green) and 4μM EthD-1 (dead/red) after 24 hours in culture. All controls contain no plasminogen. Images taken using 10x and 20x objective lens.

Thiolated fibrinogen

Due to the fact that VEGF-165 binds readily to heparin, we sought to examine crosslinking functional heparin to our fibrin microfibers, to allow rapid binding of VEGF to the microfibers. The first method is shown in the chemical schematic in Figure 7. We used a well-established thiolation [83] (sulfhydryl addition) protocol that added free thiols to the primary amines of fibrinogen using Traut's reagent, which is a cyclic thioimidate. The compound is beneficial because it only adds a small spacer arm with a

terminal sulfhydryl group and it largely maintains the charge properties **(Fig. 7A.)** Additionally, the thiols react readily with free methacrylate groups, and it is what we used to conjugate the fibrinogen to the heparin methacrylate.

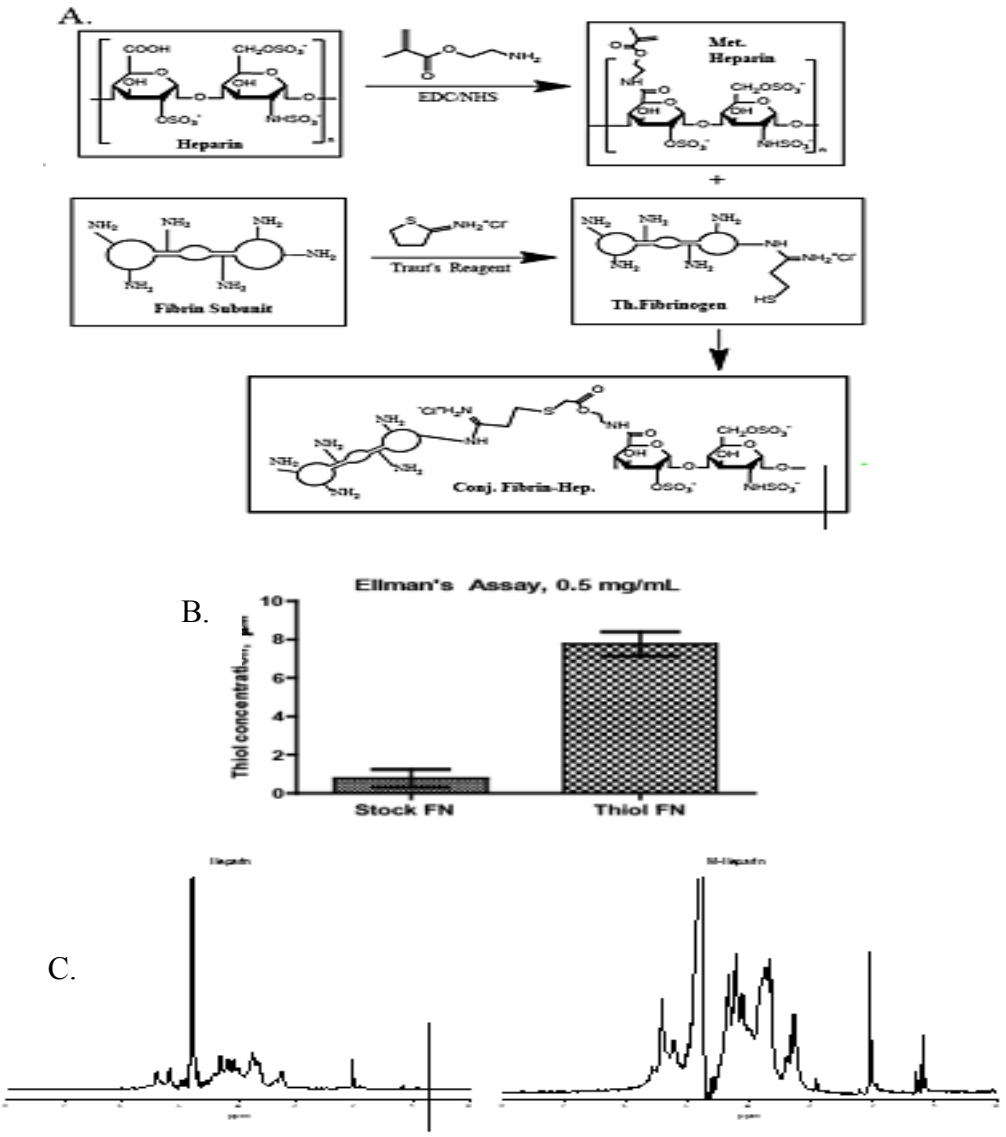

Figure 7. Heparin methacrylate and thiolated fibrinogen crosslinking with relative assays. (A) The schematic for the EDC/NHS/AEMA heparin methacrylation protocol, the Traut's reagent based thiolated fibrinogen, and the crosslinking of both. (B) The Ellman's Assay of free thiols present in a 0.5 mg/mL solution containing modified fibrinogen in distilled water. n=4 with quadruplicate wells (C) ^{1}HNMR peaks of methacrylated heparin and the unmodified heparin control. The heparin was solubilized to 10 mg/mL in D_2O.

Despite Traut's reagent's ability to relatively maintain constant charge at the addition site, we found that as the reaction proceeds, the solubility of the fibrinogen decreases significantly. However, we believed the introduction of heparin would help the solubility of the fibrinogen-heparin complex. Due to the insolubility, ^{1}HNMR in an aqueous solvent was not possible. We employed Ellman's Assay, a UV spectrophotometer based method that detects and quantifies free thiols. The Ellman's reagent reacts with free thiols, cleaving the disulfide bond to yield TNB^- (3-thio-6-nitrobnenzoate) which becomes TNB^{2-} in basic solutions. The UV spectrophotometer detects created TNB^{2-} due to its yellow color. We had to use a small concentration of thioliated fibrinogen (0.5mg/mL) due to its large insolubility. At this concentration, **Figure 7B** shows that 7.77 μM of free thiols are present in the thiolated fibrinogen compared to 0.78 μM for the stock fibrinogen control. We completed the calculation of free thiols using three data points for separate batches, for a total of six data points for both the experimental and control. The governing equations are

$$\Delta A_{FreeThiols} = A_{sample} - \left(\frac{3.1}{3.2}\right)\left(A_{DTNB} - A_{buffer}\right) \quad \text{[Equation 1]}$$

$$[free\ thiols] = \frac{\Delta A_{FreeThiols}}{\varepsilon\lambda} \quad \text{[Equation 2]}$$

where ε is the extinction coefficient equal to 1.415 x 10^4 $M^{-1}cm^{-1}$, λ is the experimental wavelength equal to 412 nm, and A is the UV spectrophotometer absorbance at 412 nm. The free thiol concentration is derived from Beer-Lambert's Law.

Methacrylated heparin

In order to crosslink with the thiolated fibrinogen, we had to add methacrylate groups to heparin sodium salt. Heparin is easily methacrylated using common EDC/NHS

chemistry, and the protocol is documented in Jeon et al. In this schematic, the methacrylated heparin is synthesized by the methacrylation of the two carboxylic acid groups. Heparin is found to contain linear chains of repeating disaccharide units. The most common disaccharide is 2-O-sulfated iduronic acid and 6-O-sulfated, N-sulfated glucosamine, IdoA(2S)-GlcNS(6S). The **Figure 7A** schematic shows this most common repeating unit, and is the focus of the methacrylation chemistry. We covalently linked the aforementioned main chains of heparin using the carboxylic acid reactive groups and the amines of the AEMA. The AEMA reacting with carboxylic acid forms stable amide linkages using common EDC/NHS chemistry.

We employed ^{1}HNMR to detect the specific peaks for methacrylated heparin. We created curves for both stock heparin and our generated methacrylated heparin. There are three main curves for the detection of methacrylated heparin. The first peaks are located at 5.8 and 6.2 ppm and these peaks correspond to the second carboxyl group. The 2.9 ppm curve is correlated with the terminal carbon. The final curve, located at 1.9 ppm, shows the presence of the first carbon after the primary amine added through AEMA addition. As shown by our experimental ^{1}HNMR curve, there are distinctly new peaks at the 1.9 and 2.9 ppm point. However, the 5.8 and 6.2 ppm curves are not clear **(Fig. 7C.)** Despite the lack of curves at this region, these peaks are known to be the less substantial of the three main points.

Crosslinking and cell viability

For a successful material, the heparin and fibrin must readily crosslink to each other while maintaining many of the same properties of the stock fibrinogen. Two such properties are cell biocompatibility and material solubility. First, the material failed to

maintain the desired solubility. For stock fibrinogen, 2.0 wt% is easily achievable with slight increase in temperature (37°C) and minimal ultrasonication. At 2.0 wt%, we can create proper electrospun fibers for our experiments. However, we could only achieve a concentration of 0.10 wt. % before significant cloudiness and aggregation. This concentration was too low for electrospinning, and the highly insoluble concentrations were not suitable for the even flow patterns desirable through small gauge needles.

Despite solubility concerns, we wanted to test the crosslinking of the heparin methacrylate and fibrinogen in 2D conditions where solubility has less bearing on the 2D sheet. The crosslinking mechanism and final product is shown in **Figure 7A**.

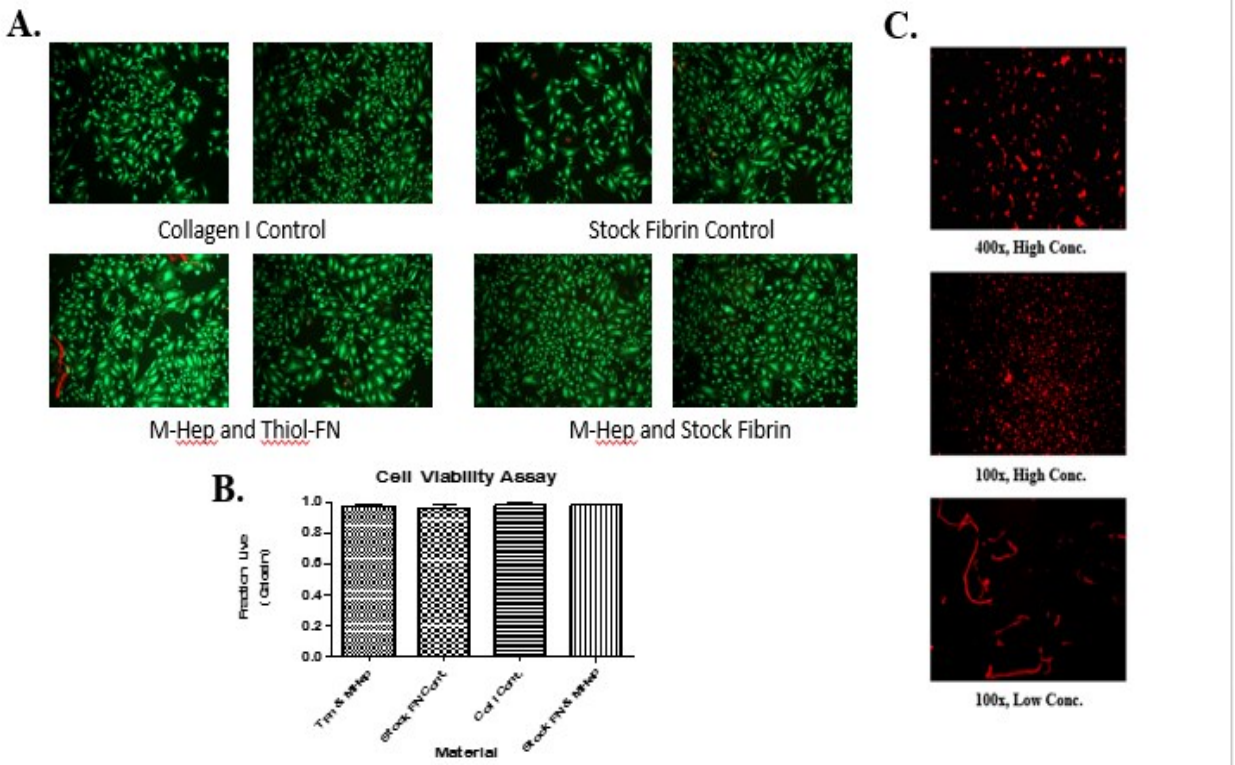

Figure 8. Cell viability and crosslinking testing of methacrylated heparin-thiolated fibrinogen system. (A) 2D fluorescent images of ECFCs seeded on coverslips coated in a variety of materials. The cells are stained with 2µM calcein (live/green) and 4µM EthD-1 (dead/red) after three days in culture. (B) Live cells were manually counted using Image J and plotted as a percentage of total cells on the coverslips. We used the images from (A) for the graph in (B). n=2 for quadruplicates. (C) 2D fluorescent images of thiolated fibrinogen with thrombin coated coverslips coupled with Dylight Rapid Link 550 labeled methacrylated heparin. Low concentration is 0.2% fibrinogen, high concentration is 1.0% fibrinogen. The control was stock fibrinogen and showed no clear binding/fluorescence.

To test crosslinking, we fluorescently labeled heparin using the Lightning-Link Rapid DyLight 550 kit. Fluorescently-labeled heparin and fibrinogen were added in a thin layer to the 2D culture dish followed by thrombin crosslinking. After multiple washes, all heparin bound regions of fibrin were visible under fluorescent microscopy at 550nm. The control was stock fibrinogen with the labeled heparin. The control showed minimal red fluorescent background with no clearly bound heparin-fibrin regions, as expected. The thiolated fibrinogen showed clear fluorescent crosslinking, and the images are displayed above in **Figure 8C**. Due to the aforementioned insolubility, the high concentration shows regions of fibrin clumping, whereas the more soluble low concentration forms the fibrils more common to stock fibrin 2D mesh.

The newly created growth-factor delivery material must be biocompatible for future experiments and cell testing. The most common and sensitive cells used in our project are ECFCs. We seeded ECFCs on the 2D fibrin-heparin sheets to determine the cell viability of our material. We used live-dead (calcein/EthD-1) stain testing on five day ECFC cultures on the new heparin-fibrin material, a stock fibrin and stock heparin control, Col I control, and a stock fibrin with methacrylated heparin control. As shown by **Figure 8B**, there is no significant difference between live cell percentage of the controls and the newly created material. We show in **Figure 8A**, that the cell morphology is roughly unchanged between our controls and experimental coating.

Reductive amination for direct heparin-fibrinogen crosslinking

We determined that individually modifying heparin and fibrinogen led to problems upon crosslinking. Fibrinogen is somewhat insoluble in its stock form and the

addition of sulfhydryl groups lead to further insolubility. The lyophilized thiolated fibrinogen aggregated upon addition to any aqueous solution, thereby secluding the free thiol groups from dissolved metyhacrylated heparin. The heparin could not penetrate the aggregate core of the fibrinogen to increase the overall solubility of the fibrinogen. Therefore, we needed to directly crosslink heparin and fibrinogen simultaneously in order to alleviate any solubility concerns.

We modified a reductive amination protocol used for grafting hyaluronic acid (HA) to fibrinogen outlined in Yang et al. In our process, we employ $NaCNBH_3$ as the reducing agent. The reaction is best carried out in a basic buffer ($Na_2B_4O_7$/NaCl, pH 8.0), which is optimal for reductive amination using $NaCNBH_3$. The addition of the sodium cyanoborohydride caused the reduction of Schiff's base (**Fig. 9**.)

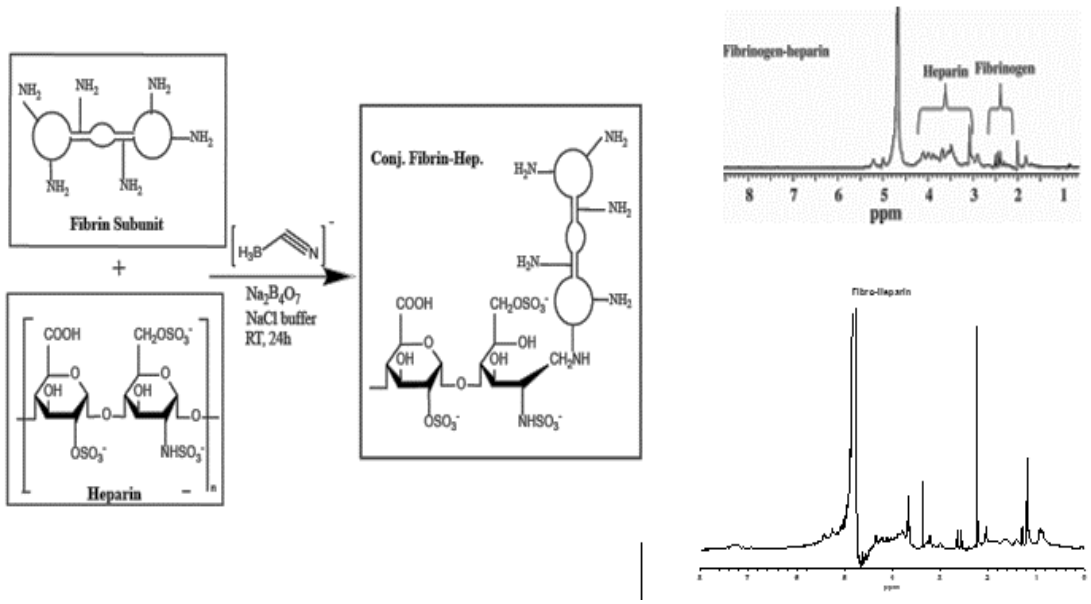

Figure 9. Schematic of reductive amination protocol with corresponding ^{1}HNMR.
The schematic is an outline of crosslinking heparin with fibrinogen subunits using reductive amination. The top ^{1}HNMR curve is the theoretical curve from Yang et al with labeled heparin and fibrinogen regions. The bottom ^{1}HNMR curve is the experimental curve derived using 10 mg/mL in D_2O. [81]

To test the crosslinking between the heparin and fibrinogen, we used ^{1}HNMR. For conjugated heparin and fibrinogen, we expect the curve exhibited in **Figure 9**, as described in Yang et al. The specific region for heparin is found between 4.3 and 3.1 ppm and 2.6 and 2.1 ppm for fibrinogen. Our experimental NMR curves show the expected curves in this region. However, at the 2.1 ppm to 1.0 ppm range, there are significant curves, which are most likely due to some leftover reagent, even after filtering. [81] The fibrinogen-heparin complex is very soluble in aqueous solution, making the 3D fibrin microfibers possible with our electrospinning protocol. The final product solution has a dark brown color, but the majority of the color is removed during filtering with a 0.22 micron syringe filter. The ability to filter is beneficial for future cell work, where we can keep the entire electrospinning procedure sterile through filtering. For our current protocol consisting of drying, rehydrating, and sterilizing, the fibers seem to maintain the same physical properties as the stock fibrinogen. The addition of heparin to the stock fibrinogen forced us to use a higher concentration of fibrinogen during electrospinning to balance for the small weight percent of the heparin.

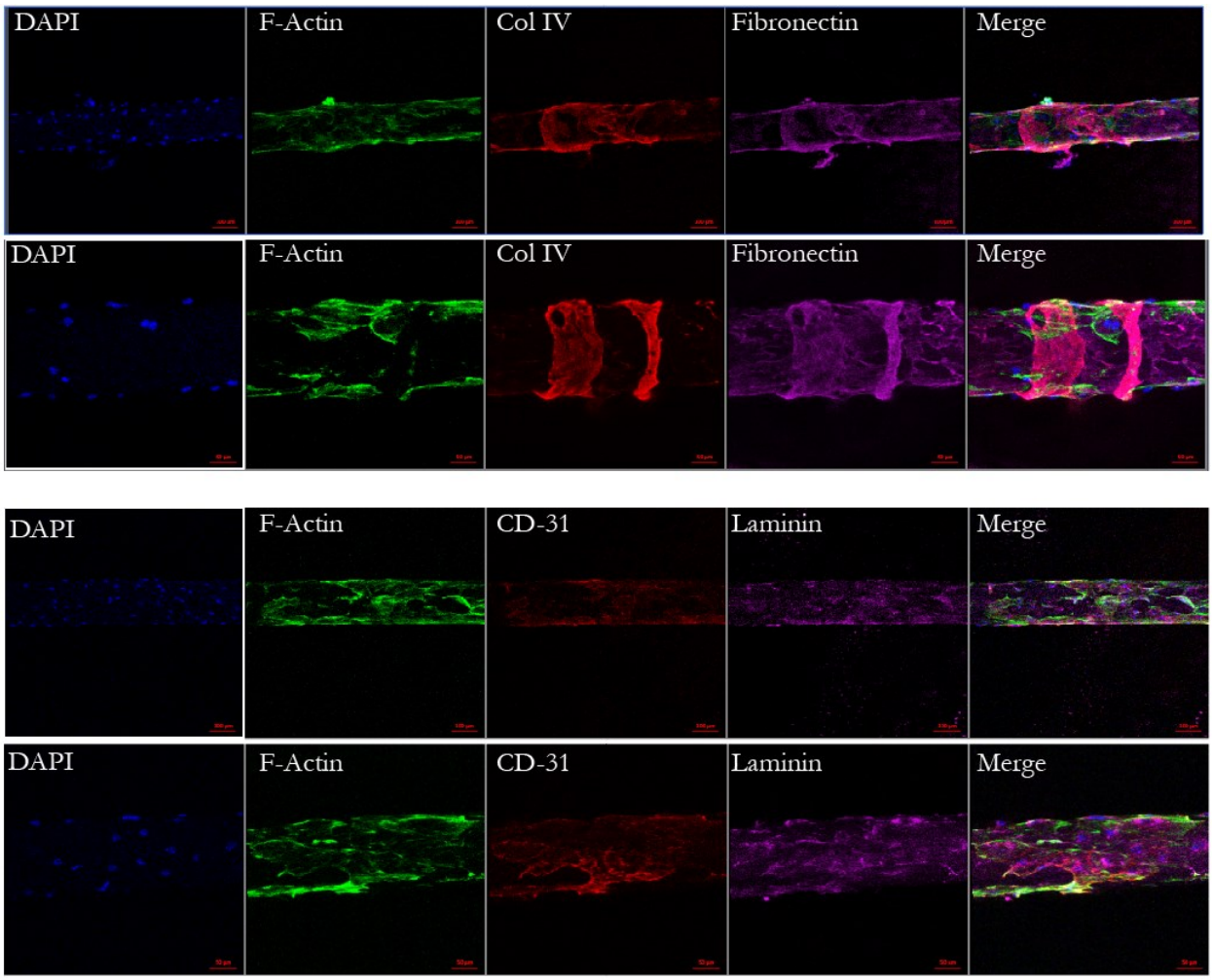

Figure 10. ECFCs seeded on 3D VEGF bound Hep-Fibrinogen fibers with ECM deposition. Confocal z-stack projections of ECFCs cultured on reductive amination derived Hep-F electrospun fibers. VEGF was initially bound to the fibers before proceeding with cell culture for five days. The top image in each set used the 10x objective lens and the bottom 20x objective. The scale bar for low magnification was 100 µm and 50 µm for the high magnifications. The ECM is stained in magenta and red, F-actin in green, and nuclei in blue. n=2 with duplicates.

Cell biocompatibility of VEGF bound fibrin microfiber

Our previous experiments have shown that the lack of VEGF supplements (50 ng/mL) in the standard ECFC media hinders the formation of visible ECM deposited on the 3D microfibers. We wanted to show that VEGF bound to heparin in our experimental

microfibers would produce significant ECM in non-supplemented media. For the initial experiment, we added VEGF-supplemented media and two million cells to each fiber for 12 hours, after which we cultured the cells in normal VEGF media for five days. Additionally, we wanted to the study the orientation of the cells (F-actin) and the ECM in relation to the microfiber, similarly to the stock fibrinogen. In **Figure 10**, we show that collagen IV, fibronectin, and laminin are deposited by ECFCs on the heparin bound microfiber. Additionally, F-actin looks to align with the fiber in most cases and the cells form a continuous layer on the microfiber, speaking to its biocompatibility. The F-actin seems to be slightly more disorganized than the control, but still mostly aligned with the longitudinal axis of the fiber. Similarly to the stock fibrin control, the collagen IV and fibronectin clearly align perpendicular and circumferentially wrap the fiber. Additionally, the CD-31 marker is clearly visible at the cellular junctions, showing the presence of a mature endothelium. The laminin is visible, but the organization and alignment is indeterminate. The higher magnification images seem to suggest alignment in the direction of the fiber's nanotopography.

ELISA Assay for VEGF release profile

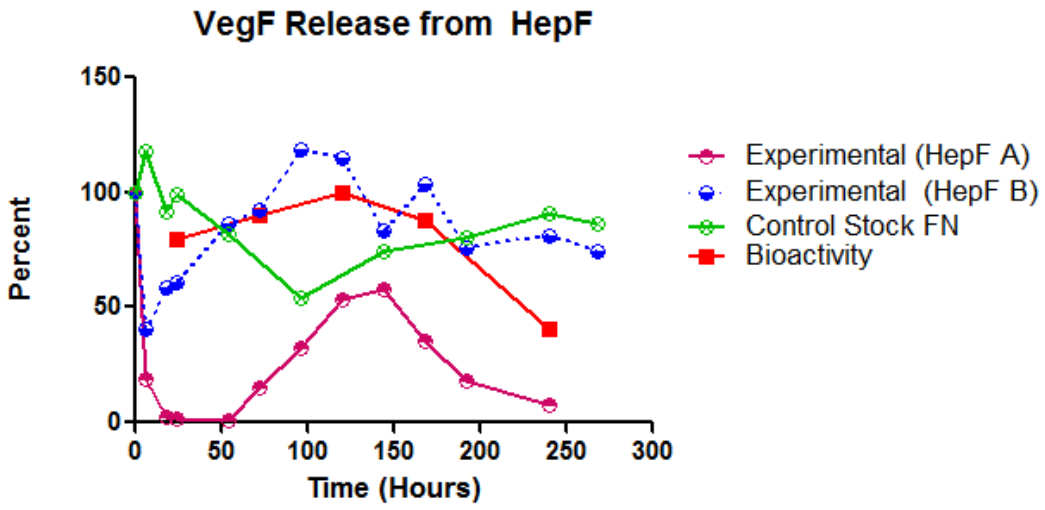

Figure 11. VEGF release from heparin-bound fibrin fibers. The release of VEGF from 3D modified heparin fiber in a 12 well culture plate at 37C for 250 hours. Experimental corresponds to n=2 of modified heparin, while the control is unmodified fibrin fibers. The bioactivity is the degradation of VEGF activity over the experimental time.

In order to test the release profile of VEGF bound to our modified fibrin fiber, we utilized ELISA assay to quantify the amount of VEGF in solution after release from the fiber. At time zero, the detected VEGF concentration is considered 100% for all samples. For both of the modified heparin, there was an initial decrease in solution VEGF concentration before releasing close to 50% of total VEGF by 150 hours. The bioactivity of VEGF is shown to decrease by a factor of two over the course of the experiment. Control fibrin shows a relatively constant VEGF concentration in solution indicative of minimal VEGF binding by fibrin.

DISCUSSION

We strived to develop an organic, evolving 3D fibrin-based microfiber for the study of vascular ECM in vitro. As previously mentioned, the ECM produced by all angiogenic cell types is integral to the development and integrity of blood vessels in vivo. The organization of this ECM differs significantly depending on the vessel size, type and function. For example, postcapillary venules range from 10 to 30 μm consisting of endothelial cells with a capillary-like semi-permeable layer of pericytes. Venules greater than 50 μm in diameter exhibit a thin adventitia with a smooth muscle layer. Arterioles, closer to the size of our fibers, in the range of 100 to 300 μm in diameter show an aligned endothelial cell layer in the direction of blood flow, similar to the 300 μm to one centimeter muscular arteries.

For the vessels being modeled by our fibrin system, a well-defined fenestrated internal elastic membrane sits on a layer of aligned endothelium. Above this layer sits a fully-developed tunica media consisting of circumferentially oriented endothelial cell produced ECM in addition to vSMCs. The majority of the ECM is composed of collagen and elastic fibrils, but other ECM proteins, such as fibronectin and lamin, are largely unstudied. The circumferentially aligned fibrils are believed to allow the constant constriction and expansion of vessels when prompted by chemical or neural signals. However, this organization has only been truly viewed in the media layer, whereas the tunica intima alignment is largely unknown. This relatively small layer is difficult to view in vivo with current laboratory techniques. The minimal published data suggests a mixture of both axial and circumferential alignment with more circumferential orientation close to the lumen. This alignment mixture is intuitive because the axial alignment

provides increased tensile strength and resistance to the blood flow's shear stresses. The circumferential alignment provides the necessary strength to counteract the contractile stress due to the distending pressure of blood flow. This duality of stresses indicates the need for both the circumferential and axial alignment in vasculature and vessel models. However, current models fail to provide a platform for the generation of both forms of ECM and multiple layers of vSMCs. Our fibrin model provides the specific nanotopography necessary for the generation of these orientations, and allows us to view the deposition and organization of a variety of ECM components, including the unstudied components like laminin and fibronectin.

Our model is novel because it allows us to visualize both the cellular and ECM organization under nanotopographical cues. The fibrin microfiber model allows to better understand the microvasculature deposition, development, and organization and better apply that knowledge to future in vivo and regenerative medicine applications. The current approaches in creating 3D microvasculature models tend to utilize hydrogels, scaffolds with imbedded vascular cells, and micropatterned devices to study organized microvasculature structures. These models are successful in studying spontaneous vessel formation and processes, they fail to provide the direct topographical cues that mimic ECM based cues in vivo. Therefore, our model looked to create a model with proper ECM organization that can investigate multi-cellular interactions and structures in vitro.

The fibrin model we developed creates a natural progression from early stage endothelial and ECM formation to a more complex model for angiogenesis. Our first goal was to demonstrate the effectiveness of the 3D fibrin construct. Our previously described electrospinning and stretching process created the novel line-grating

nanotopography integral to the overall experiment. The topography was shown to allow endothelial cell organization and the subsequent co-culture of support mural cells, i.e. vSMCs. The initial study focuses on fibers centered at a 150 μm diameter. These diameters are known to represent venules and arterioles, which are largely unstudied in previous research. The specific topography allow us to focus on the poorly unstudied ECM proteins deposited by endothelial cells, as most studies utilize a pre-generated, decellularized ECM. We successfully cultured ECFCs on these microfibers and the ECFCs formed a contunous monolayer over the length of the fiber. The ECFCs after five days also exhibited the more elongated morphology indicative of mature endothelial cells. The ability to mount the ECFCs directly on top of the electrospun fiber, and not directly interwoven within the electrospun mesh, is a unique result. Therefore, the surface of the fiber provides detailed control over the endothelial layer.

Our primary studies imaged and characterized the ECM produced by ECFCs seeded directly on the fibrin microfiber. We showed that after five days in culture, the ECFCs deposited collagen IV, fibronectin and laminin, all of which exhibited circumferential wrapping. This ECM wrapped perpendicular to the longitudinal axis of the fiber. Additionally, the F-actin, and therefore the cells themselves, were shown to align in the direction of the fiber and the overall nanotopography. The ECM produced in the five culture days was completed in the presence of VEGF supplemented media to spur ECM production. Additionally, ECFCs were utilized because they are known to deposit abundant ECM. It is also important to note that after longer ECFC culture periods (longer than ten days) the ECM formed multiple layers on the fibrin with complete and continuous coverage of the microfiber. This data is not shown because

after these longer culture periods, the large amounts of produced ECM obscure the orientation of individual fibrils. Due to these long-term imaging concerns, we limited our studies to five days for ECFC culture, but have witnessed cell survivability over longer culture periods.

Our main hypothesis is the aligned nanotopography is the greatest factor in determining the deposition and alignment of the ECFC produced ECM. By using two models—2D fibrin sheets and 3D PES fibers—we determined ECM alignment was a result of both the fiber geometry coupled with the fibrin topography. The flat fibrin sheet possess the same nanotopography as the 3D fibers, but lacked the same shape and geometry. The cells seeded on these 2D frames similarly aligned with the topography of the fibrin sheets, as shown by the F-actin staining. However, the ECM alignment was random and did not organize circumferentially, suggesting the importance of fibrin geometry on our study. To test the importance of the specific nanotopography, we generated a 3D PES control with a fibrin coating to ensure ECFC biocompatibility but lacked the aligned topography. Instead, the fibrin coating created a completely random orientation of the PES material. The ECFCs and F-actin no longer aligned with the PES fiber but still produced a circumferentially aligned ECM. This result suggests cell alignment is induced by fiber topography, but the ECM alignment is controlled by fiber geometry. The random cell alignment on PES, in addition to a previous study that disrupted the cellular cytoskeleton, allows us to conclude the ECM alignment is ultimately independent of cellular orientation.

Once we determined ECM organization is regulated by 3D geometric sensing, we wanted to define the major geometric characteristic of this regulation. To date, no study

has shown the importance of curvature to cell generated ECM at the microscale, especially during microvascular creation and organization. We hypothesized the driving force of ECM organization is curvature sensing, or more specifically the fibrin microfiber diameter. We are able to control the diameter of our fibers through three major parameters: stretching percent, spin time, and initial fibrin loading. We created fibers ranging in size from 100 to 500 μm by altering the electrospinning time. Spin time was the best parameter to use because altering the stretching parameters would alter the fiber's nanotopography and an increased fibrinogen concentration could affect the overall mechanical and biological properties of our model. The study showed that once the fiber diameter exceeded 400 μm, the ECM lost circumferential orientation. At that point, the ECM organization exhibited randomness, the same randomness seen in the 2D fibrin sheet control. The effect of curvature has yet to be reported in other research studies, and speaks further to the novelty of our model. Despite elucidating the importance of curvature on ECM organization, we have yet to determine the underlying mechanism that drives this response.

The importance of this model is the ability to modify different aspects in order to mimic and understand more complex interactions. One such advancement of the model is the ability to co-culture mural cells, more specifically vSMCs, on the ECFC and ECM layer. We were able to seed a complete layer of vSMCs on top of ECFCs while simultaneously studying the ECM produced by these vSMCs. We determined the vSMCs produce a variety of ECM orientations on the endothelial layer, from complete randomness to circumferential wrapping. One unique aspect of the vSMC's ECM deposition is the ECM is stacked in multiple layers, different from the ECM monolayer

deposited by the ECFCs. According to published data, the vSMC ECM typically align circumferentially to the vessel in order to maintain the necessary contractile strength for maintaining blood flow in vivo. We fail to witness this orientation, but it is believed that the vSMC ECM wrapping is prompted in the presence of blood flow. The lack of blood flow in our system produces a model most closely representing muscular venules, which have much lower blood pressures than arterioles in vivo. Muscular venules are found to contain randomly oriented vSMCs for this reason.

We have clearly shown the effectiveness of our model, and we wanted to further develop the 3D fibrin microfiber platform. As previously mentioned, we must supplement the media with a higher concentration of VEGF in order to produce a more robust, semi-continuous ECM. However, a system where VEGF is directly bound to the culture scaffold is more effective than aqueous VEGF. Previous studies have shown that bound growth factor allows for a more controlled dose over a longer time period administered directly to the cellular layer. The dosage over time improves the functionality of the model, especially for future in vivo implantation and for an autonomous in vitro system. In vivo, a high concentration of aqueous VEGF can lead to uncontrolled and spontaneous angiogenesis in the healthy surrounding tissue. One concern of regenerative medicine researchers in the negative effects of high growth factor doses due to their implants, including the formation of cancerous tumors.

Presently, there are no effective protocols for binding VEGF to fibrinogen that allow for electrospinning into the 3D microfibers used in our study. Due to concerns over the solubility and charge dependence of our electrospinning process, we tested two different protocols for crosslinking heparin to fibrinogen, as heparin is known to directly

bind VEGF and is suitable for a controlled release. Additionally, heparin is known to have a low surface charge and good solubility in aqueous solutions, making it ideal for our processes.

The first method attempted to crosslink thiolated fibrinogen with methacrylated heparin, which is well-known and established approach. We determined that free thiols are added to the primary amines of fibrinogen using Traut's reagent. We initially determined that Traut's reagent was the best option for thiolation because it maintains constant charge at the free thiol site. This is ideal because the success of the electrospinning process and ultimately the mechanical properties of the fiber are largely dependent on the surface charge. A change in surface charge can greatly affect the solubility as well. As the reaction proceeds, the fibrinogen lost solubility and started to aggregate out of solution, mostly due to the exposed sulfhydryl group. However, the addition of the highly soluble methacrylated heparin should significantly increase the solubility of the heparin conjugated fibrinogen. The methacrylation of heparin utilized a published protocol using AEMA and EDC/NHS chemistry to great effect. The ^{1}HNMR shows a significant addition of methacrylate groups and the success of the protocol. Unfortunately, the addition of heparin did not improve the solubility of the fibrinogen. We believe the exposed carboxyl group after crosslinking leads to the observed insolubility. Another potential explanation is the aggregation of thiolated fibrinogen buries the free thiols within the aggregate due to the hydrophobic affect. If this is the case, there may be an insufficient number of free thiols to bind enough methacrylated heparin molecules for improved solubility. To prevent rapid aggregation during material

preparation, we needed to design a protocol that simultaneously modifies and crosslinks both heparin and fibrinogen.

Even with solubility concerns, it was important for us to show that heparin-conjugated fibrinogen is suitable for future cell culture and ECM orientation studies. First, we proved that heparin successfully binds to fibrinogen using a fluorescently labeled heparin. Multiple iterations of washing failed to remove fluorescently-labeled heparin, indicating successful binding to thrombin catalyzed thiolated fibrin gels. This study also imaged the organization of the fibrin layers compared to the stock fibrin after thrombin addition. The lack of solubility seems to prevent the formation of fibrils typically seen in the formation of 2D coated coverslips. Additionally, the fibrin layers were uneven with regions of higher fibrin concentration. These changes to fibrin crosslinking led us to forgo further testing of this material because uneven concentration of fibrin solutions during electrospinning causes irregular and weak regions in the 3D microfiber. Also, aggregates in the fibrin solution lead to clogging in the small gauge needles used during electrospinning. We manipulated certain conditions, such as thiolation time, pH, temperature, and sonication, in an attempt to further solubilize the conjugated material. Similar to stock fibrinogen, these parameter changes fail to improve the overall solubility of the solution. Despite these setbacks, examining cell viability on the experimental 2D heparin conjugated fibrin sheets is useful for future heparin-fibrin based materials. We showed that ECFCs, the main endothelial progenitor cell type utilized in our study, predominately survive when cultured on this material. This successful biocompatibility study lends further credibility to our overall approach.

The second attempt for conjugating heparin to fibrinogen consisted of modifying a reductive amination protocol that adds stock heparin to stock fibrinogen in one, overnight step. The ^{1}HNMR curves shows the successful addition of heparin to fibrinogen, but raises other concerns as well. First, additional peaks within and outside the heparin regions indicate the presence of either unremoved reagents and byproducts or unwanted contaminants added during the highly sensitive ^{1}HNMR assay. An increased dialysis time with more vigorous mixing may lead to a purer final product. We conducted the ^{1}HNMR testing after filtering, which removed the majority of the deep brown color, but a slight brown color remained. This color corresponded to the reducing agent, $NaCNBH_3$, and suggests leftover reagent in solution. After freeze-drying, the lyophilized heparin conjugated fibrinogen generated from this protocol was extremely soluble in aqueous solutions, even more so than the stock fibrinogen. In some cases, syringe filtering (0.22 μm) causes the degradation or elimination of the target protein, but the ^{1}HNMR testing shows minimal effect on the corresponding fibrinogen peaks. The ability to filter this material provides further functionality to the material because it allows for completely sterile preparation of our electrospun fibers.

The color contamination was minimal and the solubility was sufficient enough to pursue electrospinning and cell seeding. We wanted to keep as many of the parameters used for stock fibrinogen constant with our new material. However, using the normal two percent fibrinogen in loading led to weak fibers after the alginate dissolved. Therefore, we needed to use a four percent heparin-fibrinogen solution to account for the portion of heparin when calculating solution concentration. We needed to shorten the spin time in order to maintain the proper microfiber diameter (100-200 μm) for ECFC

based experiments. The stretching percentage was maintained to preserve the integral nanotopography for cellular organization. We successfully created heparin-conjugated fibrin microfibers that could be dried, sterilized and rehydrated. We wanted to image ECFC attachment and ECM orientation on our newly formed material as we did with stock fibrin. The study showed that cells mostly aligned in the direction of the fiber with distinct F-actin organization, but seemed slightly more disorganized compared to ECFCs on the stock fibers. Additionally, collagen IV and fibronectin aligned circumferentially which again is the same for stock fibrin fibers within this diameter range. The ECFCs largely expressed CD31 at cellular junction, which shows the formation of mature endothelium after five days in culture. One difference is the deposited laminin on the new fibers failed to show any distinct organization. This suggests that of the three visualized ECM proteins, fiber curvature has the smallest effect on laminin organization. ECFC culture on these fibers allow us to draw a major conclusion, even without a conclusive ELISA-based VEGF release study—the heparin-conjugated fibrin fibers can successfully bind VEGF. The ELISA shows an initial uptake of VEGF indicative of successful binding and platform, but the later time points are inconclusive due to a loss in VEGF bioactivity, a lack of evenly mixed solution, or a constant bind-release equilibrium. Further ELISA testing with more controls and experimental fibers is necessary to fully classify our platform. Previous experiments show that ECFCs fail to generate ECM in large quantities in the presence of normal ECFC media when cultured on 3D fibrin microfibers. Ultimately, this conclusion provides further functionality and uniqueness to our overall vascular model.

CONCLUSION

We developed an important, novel, and constantly expanding in vitro model using fibrin microfibers as our base platform. The main focus of our platform was to study ECM deposition and organization on a variety of materials' properties. Each specific material attempted to guide the organization of microvascular structures by employing different curvatures and topographical alignment. We were able to align and elongate ECFCs on stock fibrin and VEGF-bound fibrin microfibers, and thereby produce a circumferential wrapping of ECM. Additionally, we successfully cultured vSMCs on the fiber's ECFC-produced endothelial layer. We determined the most important parameter for ECM organization is fiber diameter. The microfiber model is constantly evolving, including growth factor binding. For heparin-bound VEGF microfibers, we determined reductive amination is the most effective protocol for electrospinning. VEGF immobilized on the fibrin microfiber removes the need for high concentrations of VEGF in the culture media to produce significant ECM. Ultimately, we developed a constantly evolving fibrin microfiber-based model to better study the overall human microvasculature assembly. Conclusions drawn in this study may help to understand a variety of diseases and treatments integral to human health and development.

FUTURE WORK

One of the major benefits of our fibrin-based system is the option to constantly evolve the technology and manipulate key parameters. Through these additions and changes, we can study changes to ECM deposition and orientation, cell-cell interactions, growth factor responses, and overall changes to vasculogenesis and angiogenesis.

First, we can develop the interaction of growth factors and our fibrin microfibers. We need to explore the binding and release profiles, utilizing ELISA assays, of VEGF bound to our heparin conjugated fibrin. Also, previous studies have shown that other heparin-binding growth factors, such as platelet derived growth factors (PDGF), could successfully bind to our heparin-conjugated fibrin platform. We can determine if other growth factors help to proliferate mural or endothelial cells layers and the corresponding ECM proteins. The controlled release of VEGF may allow for in-vivo implementation or in-vitro culture over longer time periods. Lastly, it would be interesting to quantify any difference in ECM production by ECFCs and mural cells between the VEGF-bound fibrin and the stock fibrin microfibers. Studies show that bound growth factor may affect overall ECM production as growth factor is delivered directly to the cell layer and bound growth factor shows improved bioactivity.

Second, there are a variety of experiments to carry out on both the VEGF-bound and stock fibrin microfibers. It is important to not only study the ECM orientation, but also quantify the total ECM produced by the various cells. Comparing the quantities of ECM deposited on 2D, 3D, and various fiber diameters may help us better understand cell-produced ECM under different conditions. We can quantify the ECM produced by using qRT-PCR specific to ECM proteins. We want to explore using pericytes, not

SMCs, as the mural cell layer for our co-culture experiments. Pericytes are found in different vessel types, and may help to expand the applicability of our model to the human body. In a similar capacity, by seeding stem cells and observing the subsequent differentiation, we could study the effect of our 3D model on angiogenesis-based differentiation.

Finally, creating a microfluidic device to house and develop our fibrin microfiber could vastly improve the control we have over our system. We could create a device that immobilizes the fiber at either end with sterile media chambers for seeding and cell culture. By tethering a fiber with developed ECM to a hollow tube, we can dissolve the fibrin with plasmin and profuse media through the hollow ECM to look at contractile strength and shear stress. These in-vitro, hollow vessels are prime candidates for potential in-vivo studies. Within this microfluidic device, we can closely control parameters, like flow velocity and oxygen content, to study the effect of the surrounding environment on ECM and overall vessel development.

APPENDIX

Reagent Type	Name	Host	Vendor	Dilution	Solvent
Primary antibody	CD31	mouse	Dako	1:100	Dako antibody diluent
	vWF	mouse	Dako	1:100	Dako antibody diluent
	VEcad	mouse	Santa Cruz Biotechnology	1:100	Dako antibody diluent
	SM22	rabbit	Abcam	1:200	Dako antibody diluent
	Collagen 1	mouse	Abcam	1:500	Dako antibody diluent
	Collagen 4	mouse	Santa Cruz Biotechnology	1:100	Dako antibody diluent
	Collagen 4	rabbit	Santa Cruz Biotechnology	1:100	Dako antibody diluent
	Elastin	mouse	Abcam	1:100	Dako antibody diluent
	Fibronectin	rabbit	Sigma-Aldrich	1:100	Dako antibody diluent
	Laminin	rabbit	Abcam	1:100	Dako antibody diluent
	α-tubulin	mouse	Abcam	1:500	Dako antibody diluent
Conjugated Antibody	DAPI	NA	Roche Diagnostics	1:1000	PBS
	Alexa Fluor 488 Phalloidin	shroom	Invitrogen	1:50	Dako antibody diluent
Secondary antibody	Alexa Fluor 488 anti- rabbit IgG	goat	Invitrogen	1:1000	Dako antibody diluent
	Alexa Fluor 546 anti-mouse IgG	donkey	Invitrogen	1:1000	Dako antibody diluent
	Alexa Fluor 546 anti-rabbit IgG	donkey	Invitrogen	1:1000	Dako antibody diluent
	Alexa Fluor 647 anti-rabbit IgG	donkey	Invitrogen	1:1000	Dako antibody diluent

Appendix A. Table of antibodies and reagents used in fluorescent staining.

REFERENCES

1. Carmeliet, P & Jain, R. Angiogenesis in cancer and other diseases. *Nature*. 407, 249-257 (2000).

2. Folkman, J. in *Cancer Medicine (*eds. Holland, JF et al). 132-152 (Decker, Ontario, Canada, 2000)

3. Hanahan, D & Weinberg, RA. The hallmarks of cancer. *Cell*. 100, 57-70 (2000).

4. Bouck, N, Stellmach, V, & Hsu, SC. How tumors become angiogenic. *Adv. Cancer Res.* 69, 135-174 (1996).

5. Kerbel, RS. Tumor angiogenesis: past, present, and the near future. *Carcinogenesis.* 21, 505-515 (2000).

6. Carmeliet, P. Controlling the cellular brakes. *Nature*. 401, 657-658 (1999).

7. Senger, D & Davis, G. Angiogenesis. *Cold Spring Harbor Perspectives in Bio.* 3, 1-19 (2011).

8. Hayashi MV, Whelan MC, Senger DR. Rho Activity critically and selectively regulates endothelial cell organization during angiogenesis. *PNAS* 101, 1874-1879 (1992).

9. Hallmann, R, Horn, N, et al. Expression and function of laminins in the embryonic and mature vasculature. *Physiol Rev* 85, 979-1000 (2004).

10. Bix, G & Iozzo, RV. Novel interactions of perlecan: Unraveling perlecan's role in angiogenesis. *Microsc Res Tech.* 71, 339-348 (2008).

11. Stratman, AN, Schwindt, AE, et al. Endothelial-derived PDGF-BB and HB-EGF coordinately regulate pericyte recruitment during vasculogenic tube assembly and stabilization. *Blood*. 116, 4720-4730 (2010).

12. Akiyama, SK, Yamada, SS, et al. Analysis of fibronectin receptor function with monoclonal antibodies. *J Cell Bio.* 109, 863-875 (1989).

13. Wary, KK, Mainiero, F, et al. The adaptor protein Shc couples a class of integrins to the control of cell cycle progression. *Cell.* 87, 733-743 (1996).

14. Meredith, JE & Schwartz, MA. Integrins, adhesion and apoptosis. *Trends Cell Bio.* 7, 146-150 (1997).

15. Giancotti, FG & Ruoslahti, E. Integrin signaling. *Science.* 285, 1028-1032 (1999).

16. Ausprunk, DH & Folkman, J. Migration and proliferation of endothelial cells in preformed and newly formed blood vessels during tumor angiogenesis. *Microsvasc Res.* 14, 53-65 (1977).

17. Critser PJ, Yoder MC (2010) Endothelial colony-forming cell role in neoangiogenesis and tissue repair. Curr Opin Organ Transplant 15: 68-72.

18. Yoder MC (2009) Defining human endothelial progenitor cells. Journal of Thrombosis and Haemostasis 7: 49-52.

19. Yoder MC, Mead LE, Prater D, Krier TR, Mroueh KN, et al. (2007) Redefining endothelial progenitor cells via clonal analysis and hematopoietic stem/progenitor cell principals. Blood 109: 1801-1809.

20. Lu J, Rao MP, MacDonald NC, Khang D, Webster TJ (2008) Improved endothelial cell adhesion and proliferation on patterned titanium surfaces with rationally designed, micrometer to nanometer features. Acta Biomater 4: 192-201.

21. Bruce Alberts AJ, Julian Lewis, Martin Raff, Keith Roberts, and Peter Walter (2002) Molecular Biology of the Cell. New York: Garland Science.

22. Jain RK (2003) Molecular regulation of vessel maturation. Nature medicine 9: 685-693.

23. Hanjaya-Putra D, Bose V, et al. (2011) Controlled activation of morphogenesis to generate a functional human microvasculature in a synthetic matrix. Blood 10: 1-19.

24. Ranjan A, Webster T (2009) Increased endothelial cell adhesion and elongation on micron-patterned nano-rough poly(dimethylsiloxane) films. . Nanotechnology 20: 305102.

25. Liliensiek S, Wood J, Yong J, Auerbach R, Nealey P, et al. (2010) Modulation of human vascular endothelial cell behaviors by nanotopographic cues. Biomaterials 31: 5418-5426.

26. Bettinger CJ, Zhang Z, Gerecht S, Borenstein JT, Langer R (2008) Enhancement of In Vitro Capillary Tube Formation by Substrate Nanotopography. Adv Mater 20: 99-103.

27. Lu J, Rao MP, MacDonald NC, Khang D, Webster TJ (2008) Improved endothelial cell adhesion and proliferation on patterned titanium surfaces with rationally designed, micrometer to nanometer features. Acta Biomater 4: 192-201.

28. Bruce Alberts AJ, Julian Lewis, Martin Raff, Keith Roberts, and Peter Walter (2002) Molecular Biology of the Cell. New York: Garland Science.

29. Jain RK (2003) Molecular regulation of vessel maturation. Nature medicine 9: 685-693.

30. Schwartz SM, Benditt EP (1972) Studies on aortic intima: I. Structure and permeability of rat thoracic aortic intima. The American journal of pathology 66: 241.

31. Schriefl AJ, Zeindlinger G, Pierce DM, Regitnig P, Holzapfel GA (2012) Determination of the layer-specific distributed collagen fibre orientations in human thoracic and abdominal aortas and common iliac arteries. Journal of The Royal Society Interface 9: 1275-1286.

32. Tsamis A, Krawiec JT, Vorp DA (2013) Elastin and collagen fibre microstructure of the human aorta in ageing and disease: a review. Journal of The Royal Society Interface 10.

33. CANHAM PB, FINLAY HM, DIXON JG, BOUGHNER DR, CHEN A (1989) Measurements from light and polarised light microscopy of human coronary arteries fixed at distending pressure. Cardiovascular research 23: 973-982.

34. Finlay H, McCullough L, Canham P (1995) Three-dimensional collagen organization of human brain arteries at different transmural pressures. Journal of vascular research 32: 301-312.

35. Movat HZ, Fernando NVP (1963) The fine structure of the terminal vascular bed I. Small arteries with an internal elastic lamina. Experimental and Molecular Pathology 2: 549-563.

36. Hibbs RG, Burch GE, Phillips JH (1958) The fine structure of the small blood vessels of normal human dermis and subcutis. American Heart Journal 56: 662-670.

37. Fernando NV, Movat HZ (1964) The fine structure of the terminal vascular bed: II. The smallest arterial vessels: Terminal arterioles and metarterioles. Experimental and Molecular Pathology 3: 1-9.

38. Halloran BG, Davis VA, McManus BM, Lynch TG, Baxter BT (1995) Localization of Aortic Disease Is Associated with Intrinsic Differences in Aortic Structure. Journal of Surgical Research 59: 17-22.

39. Miller JS, Stevens KR, Yang MT, Baker BM, Nguyen D-HT, et al. (2012) Rapid casting of patterned vascular networks for perfusable engineered three-dimensional tissues. Nat Mater 11: 768-774.

40. Zheng Y, Chen J, Craven M, Choi NW, Totorica S, et al. (2012) In vitro microvessels for the study of angiogenesis and thrombosis. Proceedings of the National Academy of Sciences 109: 9342-9347.

41. Neumann T, Nicholson BS, Sanders JE (2003) Tissue engineering of perfused microvessels. Microvascular Research 66: 59-67.

42. Yee D, Hanjaya-Putra D, Bose V, Luong E, Gerecht S (2011) Hyaluronic Acid Hydrogels Support Cord-Like Structures from Endothelial Colony-Forming Cells. Tissue Engineering Part A: Mary Ann Liebert, Inc. pp. 1351-1361.

43. Hanjaya-Putra D, Yee J, Ceci D, Truitt R, Yee D, et al. (2010) Vascular endothelial growth factor and substrate mechanics regulate in vitro tubulogenesis of endothelial progenitor cells. Journal of cellular and molecular medicine 14: 2436-2447.

44. Meyer GT, Matthias LJ, Noack L, Vadas MA, Gamble JR (1997) Lumen formation during angiogenesis in vitro involves phagocytic activity, formation and secretion of vacuoles, cell death, and capillary tube remodelling by different populations of endothelial cells. 249: 327-340.

45. Bayless KJ, Davis GE (2002) The Cdc42 and Rac1 GTPases are required for capillary lumen formation in three-dimensional extracellular matrices. Journal of Cell Science 115: 1123-1136.

46. Bayless KJ, Salazar R, Davis GE (2000) RGD-Dependent Vacuolation and Lumen Formation Observed during Endothelial Cell Morphogenesis in Three-Dimensional Fibrin Matrices Involves the Integrins. The American journal of pathology 156: 1673-1683.

47. Grant DS, Tashiro K-I, Segui-Real B, Yamada Y, Martin GR, et al. Two different laminin domains mediate the differentiation of human endothelial cells into capillary-like structures in vitro; 1989 Feb 08. Cell Press. pp. 933-943.

48. Sacharidou A, Stratman AN, Davis GE (2011) Molecular mechanisms controlling vascular lumen formation in three-dimensional extracellular matrices. Cells Tissues Organs 195: 122-143.

49. Davis GE, Camarillo CW (1996) An alpha 2 beta 1 integrin-dependent pinocytic mechanism involving intracellular vacuole formation and coalescence regulates capillary lumen and tube formation in three-dimensional collagen matrix. 224: 39-51.

50. Kim DJ, Martinez-Lemus L, Davis GE (2013) EB1, p150Glued and Clasp1 control endothelial tubulogenesis through microtubule assembly, acetylation and apical polarization. Blood.

51. Hanjaya-Putra D, Bose V, Shen Y-I, Yee J, Khetan S, et al. (2011) Controlled activation of morphogenesis to generate a functional human microvasculature in a synthetic matrix. Blood 118: 804-815.

52. Lutolf M, Hubbell J (2005) Synthetic biomaterials as instructive extracellular microenvironments for morphogenesis in tissue engineering. Nature biotechnology 23: 47-55.

53. Moon JJ, Saik JE, Poché RA, Leslie-Barbick JE, Lee S-H, et al. (2010) Biomimetic hydrogels with pro-angiogenic properties. Biomaterials 31: 3840-3847.

54. Hielscher AC, Qiu C, Gerecht S (2012) Breast cancer cell-derived matrix supports vascular morphogenesis. American Journal of Physiology - Cell Physiology 302: C1243-C1256.

55. Soucy PA, Romer LH (2009) Endothelial cell adhesion, signaling, and morphogenesis in fibroblast-derived matrix. Matrix Biology 28: 273-283.

56. Pham QP, Sharma U, Mikos AG (2006) Electrospinning of polymeric nanofibers for tissue engineering applications: a review. Tissue Eng 12: 1197-1211.

57. Kumbar SG, James R, Nukavarapu SP, Laurencin CT (2008) Electrospun nanofiber scaffolds: engineering soft tissues. Biomed Mater 3: 034002.

58. Aper T, Schmidt A, Duchrow M, Bruch HP (2007) Autologous Blood Vessels Engineered from Peripheral Blood Sample. European Journal of Vascular and Endovascular Surgery 33: 33-39.

59. Gui L, Muto A, Chan SA, Breuer CK, Niklason LE (2009) Development of decellularized human umbilical arteries as small-diameter vascular grafts. Tissue engineeringPart A 15: 2665-2676.

60. Swartz DD, Russell JA, Andreadis ST (2005) Engineering of fibrin-based functional and implantable small-diameter blood vessels. American Journal of Physiology-Heart and Circulatory Physiology 288: H1451-H1460.

61. Kaushal S, Amiel GE, Guleserian KJ, Shapira OM, Perry T, et al. (2001) Functional small-diameter neovessels created using endothelial progenitor cells expanded ex vivo. Nature medicine 7: 1035-1040.

62. Cho S-W, Lim SH, Kim I-K, Hong YS, Kim S-S, et al. (2005) Small-Diameter Blood Vessels Engineered With Bone Marrow–Derived Cells. Annals of surgery 241: 506.

63. L'heureux N, Pâquet S, Labbé R, Germain L, Auger FA (1998) A completely biological tissue-engineered human blood vessel. The FASEB Journal 12: 47-56.

64. Baranski JD, Chaturvedi RR, Stevens KR, Eyckmans J, Carvalho B, et al. (2013) Geometric control of vascular networks to enhance engineered tissue integration and function. Proc Natl Acad Sci U S A.

65. Miller JS, Stevens KR, Yang MT, Baker BM, Nguyen DH, et al. (2012) Rapid casting of patterned vascular networks for perfusable engineered three-dimensional tissues. Nat Mater 11: 768-774.

66. Zheng Y, Chen J, Craven M, Choi NW, Totorica S, et al. (2012) In vitro microvessels for the study of angiogenesis and thrombosis. Proc Natl Acad Sci U S A 109: 9342-9347.

67. Melchiorri AJ, Hibino N, Fisher JP (2012) Strategies and Techniques to Enhance the In Situ Endothelialization of Small-Diameter Biodegradable Polymeric Vascular Grafts. Tissue Eng Part B Rev.

68. Fioretta ES, Fledderus JO, Burakowska-Meise EA, Baaijens FP, Verhaar MC, et al. (2012) Polymer-based scaffold designs for in situ vascular tissue engineering: controlling recruitment and differentiation behavior of endothelial colony forming cells. Macromol Biosci 12: 577-590.

69. Gui L, Muto A, Chan SA, Breuer CK, Niklason LE (2009) Development of decellularized human umbilical arteries as small-diameter vascular grafts. Tissue Eng Part A 15: 2665-2676.

70. Wu W, Allen RA, Wang Y (2012) Fast-degrading elastomer enables rapid remodeling of a cell-free synthetic graft into a neoartery. Nat Med 18: 1148-1153.

71. Huynh T, Tranquillo R (2010) Fusion of Concentrically Layered Tubular Tissue Constructs Increases Burst Strength. Annals of Biomedical Engineering 38: 2226-2236.

72. Lee K-W, Stolz DB, Wang Y (2011) Substantial expression of mature elastin in arterial constructs. Proceedings of the National Academy of Sciences 108: 2705-2710.

73. Barreto-Ortiz, S, Zhang, S, Davenport, M, et al. A novel in vitro model for microvasculature reveals regulation of circumferential ECM organization by curvature. *PloSONE.* (2013).

74. Yancopoulos, G, Davis, S, et al. Vascular-specific growth factors and blood vessel formation. *Nature.* 407, 242-248 (2000).

75. Rieux, A, Ucakar, B, et al. 3D systems deliverying VEGF to promote angiogenesis for tissue engineering. *J. Controlled Release.* 150, 272-278 (2011).

76. Zhao, W, McCallum, S, et al. Binding affinities of vasculare endothelial growth factors (VEGF_ for heparin-derived oligosaccharides. *Biosci Rep.* 32, 71-81 (2012).

77. Sakiyama-Elbert, S & Hubbell, J. Development of fibrin derivatives for controlled release of heparin-binding growth factors. *J. Controlled Release.* 65, 389-402 (2000).

78. Fairbrother, W, Champe, M, et al. Solution structure of the heparin-binding domain of vascular endothelial growth factor. *Cell.* 6, 637-648 (1998).

79. Jeon, O, Powell, C, et al. Affinity-based growth factor delivery using biodegradable, photocrosslinked heparin-alginate hydrogels. *J. Controlled Release.* 154, 256-266 (2011).

80. Yang, C, Chen, H, Wang, T, and Wang, Y. A novel fibrin gel derived from hyaluronic acid-grafted fibrinogen. *Biomed. Mat.* 6, 1-11 (2011)

81. Yang, HS, La, WG, Bhang, SH, et al. Heparin-conjugated fibrin as an injectable system for sustained delivery of bone morphogenetic protein-2. *Tissue Eng. Part A.* 16, 1225-1233 (2010).

82. Kusuma S, Zhao S, Gerecht S (2012) The extracellular matrix is a novel attribute of endothelial progenitors and of hypoxic mature endothelial cells. FASEB J 26: 4925-4936

83. Jue, R., et al. (1978). Addition of sulfhydryl groups to Escherichia coli ribosomes by protein modification with 2-iminothiolane (methyl 4- mercaptobutyrimidate). Biochem 17(25):5399-5405.

CURRICULUM VITAE

Matthew Davenport
47 Sycamore Street • Norwood, MA 02062 ♦ 223 W. 29th Street • Apt. 2 • Baltimore, MD 21211
mdavenp9@jhu.edu

EDUCATION

The Johns Hopkins University — **Baltimore, MD**
Master of Science Engineering in Chemical and Biomolecular Engineering — August 2014
- Thesis: *VEGF bound to heparin-conjugated, electrospun fibrin microfiber supports ECM formation and orientation on 3D, in vitro microvascular model*

The Johns Hopkins University — **Baltimore, MD**
Bachelor of Science in Chemical & Biomolecular Engineering — May 2013
- Dean's List: FA 2012, SP 2013
- Senior Design Project: *Color Indicating Test Strips for E. coli Produced Enterotoxins in Drinking Water*

EXPERIENCE

Gemstone Biotherapeutics — **Baltimore, MD**
Operations Engineer — June 2014-Present
- Development, optimization, and engineering of dextran-based wound healing hydrogel
- Incubating core technology from Johns Hopkins IP portfolio

JHU Gerecht Lab — **Baltimore, MD**
ChemBE Graduate Researcher — September 2011-2014
- Angiogenesis using biomolecular and materials engineering including growth factor delivery
- Performed mammalian cell culture, confocal imaging, and electrospinning
- 2012 Elenora Streb Muly Award for Undergraduate Research

Myriant Technologies — **Woburn, MA**
Advanced Process Engineering Intern — Summer 2013
- Developed methods for esterification and distillation of succinic acid based processes
- Contributed to fermentation and downstream processing modeling and efficiency studies (Aspen Plus)

European Molecular Biology Laboratories (EMBL) — **Grenoble, France**
Trainee, Pillai Group — Summer 2011
- 2011 Vredenburg Scholarship Recipient
- Worked with small Piwi-interacting RNAs found in mammalian germlines
- Purified antibodies for isolation and imaging of uncharacterized bovine proteins

Myriant Technologies — **Woburn, MA**
Cellulosic Strain Development Intern — Summer 2010, Winter 2011, Winter 2012
- Genetic recombineering of *E. coli* to optimize succinic and lactic acid production
- Small scale (1L) fermentations (anaerobic)
- Assisted on shake-flask *Bacillus coaguluns* growth studies

PUBLICATIONS

A Novel In-Vitro Model for Microvasculature Reveals Regulation of Circumferential ECM Organization by Curvature. Barreto-Ortiz, SF. Zhang, S. **Davenport, M.** Fradkin, J. Ginn, B. Mao, H-Q. Gerecht, S. 2013. PLoS ONE 8(11): e81061. doi:10.1371/journal.pone.0081061

ACTIVITIES

Office of Undergraduate Admissions — **Baltimore, MD**
Work Study Intern — October 2010-2014

Crossover Basketball — **Baltimore, MD**
Executive Board — September 2009-2013

Pi Kappa Alpha Fraternity-Iota Tau Chapter — **Baltimore, MD**
Sergeant-at-Arms — January 2010-2013

Black and Blue Jay Newspaper — **Baltimore, MD**
Distribution Manager — September 2009-2013